

The Effect of Tidal Inflation Instability on the Mass and Dynamical Evolution of Extrasolar Planets with Ultra-Short Periods

Pin-Gao Gu

Institute of Astronomy and Astrophysics, Academia Sinica, Taipei 106, Taiwan, R.O.C.

and

Douglas N. C. Lin and Peter H. Bodenheimer

UCO/Lick Observatory, University of California, Santa Cruz, CA 95064, U.S.A.

October 31, 2018

ABSTRACT

We investigate the possibility of substantial inflation of short-period Jupiter-mass planets, as a result of their internal tidal dissipation associated with the synchronization and circularization of their orbits. We employ the simplest prescription based on an equilibrium model with a constant lag angle for all components of the tide. We show that 1) in the low-eccentricity limit, the synchronization of the planets' spin with their mean motion is established before tidal dissipation can significantly modify their internal structure. 2) But, above a critical eccentricity, which is a function of the planets' semimajor axis, tidal dissipation of energy during the circularization process can induce planets to inflate in size before their eccentricity is damped. 3) For moderate eccentricities, the planets adjust to stable thermal equilibria in which the rate of their internal tidal dissipation is balanced by the enhanced radiative flux associated with their enlarged radii. 4) For sufficiently large eccentricities, the planets swell beyond two Jupiter radii and their internal degeneracy is partially lifted. Thereafter, their thermal equilibria become unstable and they undergo runaway inflation until their radii exceed the Roche radius. 5) We determine the necessary and sufficient condition for this tidal inflation instability. 6) These results are applied to study short-period planets. We show that for young Jupiter-mass planets, with a period less than 3 days, an initial radius about 2 Jupiter radii, and an orbital eccentricity greater than 0.2, the energy dissipated during the circularization of their orbits is sufficiently intense and protracted to inflate their sizes up to their Roche radii. 7) We estimate the mass loss rate, the asymptotic planetary masses, and the semi-major axes for various planetary initial orbital parameters. The possibility of gas overflow through both inner (L1) and outer (L2) Lagrangian points for the planets with short periods or large eccentricities is discussed. 8) Planets with more modest eccentricity (< 0.3) and semi-major axis ($> 0.03 - 0.04$ AU) lose mass via Roche-lobe overflow mostly through the inner Lagrangian (L1) point. Due to the conservation of total angular momentum, these mass-losing planets migrate outwards, such that their semi-major

axes and Roche radii increase while their mass, eccentricity, and tidal dissipation rate decrease until the mass loss is quenched. 9) Based on these results, we suggest that the combined effects of self-regulated mass loss and tidally driven orbital evolution may be responsible for the apparent lack of giant planets with ultra-short periods $\lesssim 3$ days. 10) Mass loss during their orbital circularization may also have caused the planets with periods in the range $\sim 3 - 7$ days to be less massive than long-period planets which are not affected by the star-planet tidal interaction. 11) The accretion of the short-period planets' tidal debris can also lead to the surface-layer contamination and metallicity enhancement of their host stars. 12) Among the planets with periods of 1-3 weeks today, some may have migrated outwards and attained circular orbits while others may have preserved their initial eccentricity and semimajor axis. Therefore, planets with circular orbits are expected to coexist with those with eccentric orbits in this period range. 13) Gross tidal inflation of planets occurs on the time scale $\sim 10^6$ yrs after their formation for a brief interval of $\sim 10^5$ yrs. The relatively large sizes of their classical and weak-line T Tauri host stars increases the planets' transit probability. The inflated sizes of the tidally heated planets also increases the eclipse depth of such transit events. Thus, the tidal inflation and disruption of planets may be directly observable around classical and weak-line T Tauri stars.

1. Introduction

Recent searches for planets around nearby solar type stars, based on the radial velocity method, show a roughly logarithmic period distribution in the currently observed period range of 3 days to several years (Marcy et al. 2000). The absence of ultra-short-period Jupiter-mass planets with $P < 3$ days, which corresponds to an orbital semi-major axis a of 0.04 AU, appears to be real and not an observational selection effect (Cumming *et al.* 1999). The host stars of any ultra-short-period planets are expected to have large radial velocity modulations which would make them conspicuous. Close-in planets also have greater transit probabilities. The unsuccessful photometric search for transiting planets around main sequence stars in the core of the globular cluster 47 Tuc (Gilliland et al. 2001) provides more evidence for a lack of Jovian planets with ultra-short orbital periods. Thus, the cutoff in the extrasolar planets' period distribution is likely to be caused by some physical effect. For example, it has been suggested (Kuchner & Lecar 2002) that the inner disk might be hot enough to allow the magneto-rotational instability to operate and thereby is largely depleted, terminating the inward migration through planet-disk interaction and causing a lack of giant planets with orbital periods less than 3 days. In the case of 47 Tuc, most of the Jovian planets might have been expelled from their host extrasolar systems due to frequent stellar encounters in the dense stellar environment (Davies & Sigurdsson 2001), or they may have had difficulties in forming in circumstellar disks with low metallicities (Pollack et al. 1996).

In this contribution, we examine the effect of tidal interaction between ultra-short-period

planets and their host stars and explore the possibility that this physical process may have led to the apparent cutoff in the observed period distribution. This investigation is an extension of our earlier calculations of the interior structures of weakly eccentric Jovian planets at constant orbital distances under the influence of interior heating and stellar irradiation (Bodenheimer, Lin, & Mardling 2001; hereafter BLM). In these previous calculations, the interior heating is imposed to be constant in time and is uniformly distributed within the planet. BLM suggest that this heating flux may be extracted from the tidal dissipation associated with the synchronization of the planets' spin with their orbital mean motion and the circularization of eccentric orbits with small semi-major axes $a \approx 0.04$ AU. Under these assumptions, BLM show that Jovian planets can be inflated to equilibrium sizes larger than two Jupiter radii, given an adequate rate of interior heating. In the proximity of their host stars, the Roche radii of the short-period planets do not greatly exceed their physical sizes. Thus, gross inflation of any planet could lead to tidal disruption and Roche lobe overflow. We investigate this process and discuss its implications.

Mass loss induced by Roche lobe overflow may also be important for the formation of short-period planets. Shortly after the discovery of the short-period planet around 51 Peg (Mayor & Queloz 1995), we suggested that it may have been formed at a distance comparable to the orbital radius of Jupiter (several AU's), after which it migrated toward its host star (Lin et al. 1996) as a consequence of disk-planet interaction (Goldreich & Tremaine 1980; Lin & Papaloizou 1986; Takeuchi et al. 1996). The survival of the short-period planets requires the termination of their orbital evolution. Among many scenarios, Trilling et al. (1998) suggest that the size of 10^6 yr old Jupiter-mass protoplanets is more than twice that of Jupiter, so that they would overflow their Roche lobe if their orbits decayed to within ~ 0.03 AU from their host stars. Trilling et al. (1998) further postulate that the lost material flows through the L1 point and angular momentum is transferred from it to the planet's orbit, which would balance the angular momentum loss to the disk and halt the orbital decay.

In §2, we briefly recapitulate the time scale and energy dissipation rate associated with both synchronization and circularization of planetary orbits. We describe the response of the planetary envelope in §3 and describe the mass-loss flow pattern associated with Roche-lobe overflow in §4. Based on some analytic approximations, we illustrate the dynamical evolution of tidally unstable planets in terms of a sequence of stages in §5. We also present in §6 the results of numerical calculations of various models of synchronization and circularization processes. Finally, we summarize the results and discuss their implications in §7.

2. Tidal interaction between short-period planets and their host stars

The equation of relative motion between a short-period planet with a mass M_p and its host star with a mass M_* and separation r is

$$\frac{d^2\mathbf{r}}{dt^2} = -\frac{GM_t}{r^3}\mathbf{r} + \sum_{i=1}^N \mathbf{f}_i \quad (1)$$

where $M_t = M_p + M_*$, and the acceleration \mathbf{f}_i includes the relativistic potential of the host star, the contribution from other planets, and the tidal and spin distortions of the star and the planet (Mardling & Lin 2002).

2.1. Synchronization of the planet’s spin

For computational simplicity, we focus our attention in this paper on the evolution of the spin angular frequency ($\Omega_{p,*}$ for the planet and star, respectively), e , and a of one single planet in the limit that its spin and orbital axes are both parallel with the spin axis of the star. We also assume the rotational and tidal distortion of the star and the planet is approximately symmetric about the line separating them so that they do not significantly affect the orbital evolution. The only remaining contribution which can lead to angular momentum transfer and induce orbital evolution is the acceleration due to the tidal damping within the planet and the star where

$$\mathbf{f}_{p,*} = -\left(\frac{3n k_{p,*}}{Q_{p,*}}\right) \left(\frac{M_{*,p}}{M_{p,*}}\right) \left(\frac{R_{p,*}}{a}\right)^5 \left(\frac{a}{r}\right)^8 [3(\hat{\mathbf{r}} \cdot \dot{\mathbf{r}})\hat{\mathbf{r}} + (\hat{\mathbf{r}} \times \dot{\mathbf{r}} - r\boldsymbol{\Omega}_{p,*}) \times \hat{\mathbf{r}}], \quad (2)$$

where $n = (GM_t/a^3)^{1/2}$ is the mean motion of the mutual orbit of the planet and the star, and $R_{p,*}$, $k_{p,*}$, and $Q_{p,*}$ are respectively, the size, Love number, and the Q -value, of the star (subscript $*$), and the planet (subscript p) (Eggleton et al. 1998). The above expression is based on the derivation for equilibrium tides with a constant tidal lag angle.

The planet’s specific orbital angular momentum $\mathbf{h} = \mathbf{r} \times \dot{\mathbf{r}}$ changes at a rate

$$\frac{d\mathbf{h}}{dt} = \mathbf{r} \times \mathbf{f}_t \quad (3)$$

where $\mathbf{f}_t = \mathbf{f}_p + \mathbf{f}_*$. The corresponding total rate of angular momentum transfer from the spin of the planet/star to the planet’s orbit

$$\dot{J}_{p,*} = I_{p,*}\dot{\boldsymbol{\Omega}}_{p,*} = -\mu\mathbf{r} \times \mathbf{f}_{p,*} \quad (4)$$

where $\mu = M_*M_p/M_t$ is the reduced mass, and $I_{p,*} = \alpha_{p,*}\epsilon_{p,*}M_{p,*}R_{p,*}^2$ is the moment of inertia of the planet and the star, respectively. The quantity $\epsilon_{p,*}$ represents the fraction of the planet and star which participates in the tidally induced angular momentum exchange. Since gaseous planets have extensive convection zones which can be fully mixed, $\epsilon_p \simeq 1$. But, solar type stars

have shallow surface convection zones so that $\epsilon_* \sim$ a few times 10^{-2} . The coefficients $\alpha_{p,*}$ are determined by the internal structures of the planet and the star. The equation of state appropriate for Jupiter-mass planets can be approximated with a polytrope with an index 1 (Hubbard 1984), in which case, $\alpha_p = 0.26$.

If the planet's/star's spin is aligned with the orbit, we find from equations (2) and (4) that

$$\dot{\Omega}_{p,*} = \left(\frac{M_{*,p}^2}{\alpha_{p,*}\epsilon_{p,*}M_{p,*}M_t} \right) \left(\frac{9n}{2Q'_{p,*}} \right) \left(\frac{R_{p,*}}{a} \right)^3 [f_3(e)n - f_4(e)\Omega_{p,*}] + \dot{\omega}_{p,*} \quad (5)$$

$$j_{p,*} = \left(\frac{-\alpha_{p,*}\epsilon_{p,*}J_oM_{p,*}}{(1-e^2)^{1/2}M_p} \right) \left(\frac{R_{p,*}}{a} \right)^2 \left(\frac{\dot{\Omega}_{p,*}}{n} \right)_{\dot{\omega}_{p,*}=0} = \left(\frac{9J_oM_{*,p}^2}{M_pM_t} \right) \left(\frac{f_4(e)\Omega_{p,*} - f_3(e)n}{2Q'_{p,*}(1-e^2)^{1/2}} \right) \left(\frac{R_{p,*}}{a} \right)^5 \quad (6)$$

where

$$f_3(e) = \left(1 + \frac{15}{2}e^2 + \frac{45}{8}e^4 + \frac{5}{16}e^6 \right) (1-e^2)^{-6}, \quad (7)$$

$$f_4(e) = \left(1 + 3e^2 + \frac{3}{8}e^4 \right) (1-e^2)^{-9/2}, \quad (8)$$

$Q'_{p,*} = 3Q_{p,*}/2k_{p,*}$ is the modified Q-value (cf. Murray & Dermott 1999), $J_o = \mu|\mathbf{h}| = M_p(GM_t a(1-e^2))^{1/2}$ is the total angular momentum of the planet's orbit, $\dot{\omega}_p (= -\dot{I}_p\Omega_p/I_p)$ is the changing rate of planetary spin due to its structural adjustment, and $\dot{\omega}_*$ is the changing rate of spin due to angular momentum transfer, by processes such as the stellar winds, between the stars and the external medium (Dobbs-Dixon, Lin, & Mardling 2002, hereafter DLM). Although the contribution from $\dot{\omega}_p$ is generally negligible, that from $\dot{\omega}_*$ due to the stellar wind can be important for the evolution of Ω_* and a . In the limit of small e , the rate of change of the planet's angular frequency is

$$\dot{\Omega}_p = \frac{9n}{2\alpha_p Q'_p} \left(\frac{M_*}{M_p} \right) \left(\frac{R_p}{a} \right)^3 (n - \Omega_p) \quad (9)$$

which induces the planet to evolve to a state of synchronization with $\Omega_p = n$.

2.2. Circularization of the planet's orbit

Tidal friction also induces the Runge-Lenz vector, $\mathbf{e} = \dot{\mathbf{r}} \times \mathbf{h}/GM_t - \hat{\mathbf{r}}$, to change (Mardling & Lin 2002) at a rate

$$\frac{d\mathbf{e}}{dt} = \left(\frac{2(\mathbf{f}_t \cdot \dot{\mathbf{r}})\mathbf{r} - (\mathbf{r} \cdot \dot{\mathbf{r}})\mathbf{f}_t - (\mathbf{f}_t \cdot \mathbf{r})\dot{\mathbf{r}}}{GM_t} \right). \quad (10)$$

The magnitude and direction of \mathbf{e} correspond to the planet's orbital eccentricity and longitude of periape so that when averaged over an orbit, the rate of eccentricity change reduces to

$$\frac{de}{dt} = g_p + g_* \quad (11)$$

where

$$g_{p,*} = -\frac{81e}{2Q'_{p,*}} \left(\frac{M_{*,p}}{M_{p,*}} \right) \left(\frac{R_{p,*}}{a} \right)^5 \left(f_1(e)n - \frac{11f_2(e)\Omega_{p,*}}{18} \right), \quad (12)$$

$f_1(e) = (1 + 15e^2/4 + 15e^4/8 + 5e^6/64)/(1 - e^2)^{13/2}$, and $f_2(e) = (1 + 3e^2/2 + e^4/8)/(1 - e^2)^5$. In the limit of small e and nearly synchronous planetary spin, the above expression can be further reduced (Goldreich & Soter 1966) to

$$\frac{de}{dt} = -\frac{63ne}{4Q'_p} \left(\frac{M_*}{M_p} \right) \left(\frac{R_p}{a} \right)^5. \quad (13)$$

In the above equation, we only considered the planet's contribution in \mathbf{f} . When the dissipation of the planets' tide in the star is also taken into account, the damping rate is modified from the expression in equation (13) by a factor

$$\beta = 1 + \left(\frac{2Q'_p}{7Q'_*} \right) \left(\frac{M_p}{M_*} \right)^2 \left(\frac{R_*}{R_p} \right)^5 \left(9 - \frac{11\Omega_*}{2n} \right). \quad (14)$$

For planets with relatively large R_p , $\beta \simeq 1$ which indicates that the star does not significantly modify the e damping rate. If the host star has the same values of Q' and average internal density as those of the planet, its contribution would be weaker than that of the planet by a factor of R_p/R_* . However, the contribution from a very rapidly spinning host star, with

$$\Omega_* > \Omega_{pc} \equiv \frac{18f_1(e)n}{11f_2(e)}, \quad (15)$$

can reduce the total rate of e damping or even induce a net rate of e excitation with a positive de/dt (DLM).

Equations (2), (4), and (10) indicate that the evolutionary time scales for Ω and e are proportional to the magnitude of $Q'_{p,*}$. These expressions are derived using equilibrium tidal models with constant lag angles. But, in reality, the stellar tidal perturbation is likely to excite gravity and inertial waves. These waves which propagate within the planet are dissipated either through convective turbulence in its interior or radiative damping near the surface. The dissipation of the waves also leads to the deposition of angular momentum which in general leads to differential rotation. The nature of these complex processes are poorly understood and the theoretical estimates of the $Q'_{p,*}$ of Jupiter-mass planets and solar-type host stars remain uncertain (Zahn 1977, 1989; Goldreich & Nicholson 1977, 1989; Ioannou & Lindzen 1993a,b, 1994; Lubow et al. 1997; Terquem et al. 1998; Goodman & Oh 1997). Some aspects of these uncertainties are associated with how and which waves are excited and dissipated. Using a prescription for dissipation due to convective eddies, Zahn (1989) found an expression for the tidal torque which when scaled with the expression in equation (2) gives a frequency dependence for

$$Q'_p = \frac{3}{4} \frac{M_p}{M_*} \frac{n t_f}{\lambda_2} \left(\frac{a}{R_p} \right)^3 \quad (16)$$

where $t_f = [MR^2/L]^{1/3}$ is the tidal dissipation time for a convective body, and $\lambda_2 \approx 2 \cdot 10^{-2}$ when it is fully convective. But, using a slightly different prescription for the dissipation in convective eddies, Terquem *et al.* (1998) find an expression for the tidal torque which corresponds to a Q'_p which is independent of n . Even less certain is how the interior of the gaseous planets and stars may readjust after the angular momentum deposition may have introduced a differential rotation in their interior.

The theoretically determined Q_* -values using both approaches imply a slow rate for close binary stars to circularize their orbits, which is inconsistent with the observations of solar-type binary stars in stellar clusters of various ages (Mathieu 1994). Mathieu *et al.* (1992) also pointed out that a power-law function ($e/\dot{e}P^{13/3}$) provides a close fit to the slope of the observed cutoff period. Such an empirical expression would correspond to a Q' value which is independent of n . Nevertheless, the observations are equally well fitted with an index of 10/3, and an index of 16/3 cannot be ruled out.

To carry out a comprehensive analysis on the physical process associated with the dissipation of the tidal disturbance is beyond the scope of the present paper. In view of these uncertainties, we took the simplest prescription based on an equilibrium tidal model with a constant lag angle for all components of the tide. This may not necessarily be the most reliable model. All the uncertainties associated with the physical processes are contained in the Q' values and we shall parametrize our results in terms of it. For a fiducial value, we note that the Q'_p -value inferred for Jupiter from Io's orbital evolution is $5 \times 10^4 < Q'_p < 2 \times 10^6$ (Yoder & Peale 1981). With this Q'_p -value, orbits of planets with M_p and R_p comparable to those of Jupiter, and with a period less than a week, are circularized within the main-sequence life span of solar-type stars. If we use equation (16) to extrapolate from the observationally determined values for Jupiter, $Q'_p \sim 10^8$ which would imply that only systems with periods less than 3 days would be circularized within a few Gyr. But, if all planets are formed *in situ* or brought to their present location shortly after they are formed, their extended radii would enhance the rate of tidal circularization. Within the observational uncertainties, all known extrasolar planets with periods less than a week and some with periods less than two weeks have circular orbits.

With the theoretical estimate of stellar Q'_* -values ($\sim 10^8$), the time scale for orbital evolution of Jupiter-mass planets is longer than the stellar age of a few Gyr unless their orbital period is less than $\sim 8 - 9$ hours (Rasio *et al.* 1996, Marcy *et al.* 2000). But, using the observed circularization time scales as a calibration, the inferred value of Q'_* is $\sim 1.5 \times 10^5$ for the very young binary stars (Lin *et al.* 1996) and 10^6 for the mature binary stars (Terquem *et al.* 1998). In this paper, we shall adopt the observationally inferred values for $Q'_{p,*}$ and discuss the implications of our results if they are somewhat larger.

2.3. Tidal evolutionary time scales

With these values of $Q'_{p,*}$, the synchronization, circularization, and migration of the planet's orbit occurs on time scales (τ_Ω , τ_e , τ_a) which are much longer than the orbital period, and they can be obtained from the time-averaged equation of motion. In the limit of $\beta \simeq 1$, small e and nearly synchronous planetary spin,

$$\tau_{\Omega p} = \frac{\Omega_p}{|\dot{\Omega}_p|} = 0.187\alpha_p\epsilon_p \left| \frac{1 \text{ day}/(2\pi/\Omega_p)}{0.34(M_*/M_\odot)^{1/2}(0.04 \text{ AU}/a)^{3/2} - 1 \text{ day}/(2\pi/\Omega_p)} \right| \times \left(\frac{Q'_p}{10^6} \right) \left(\frac{M_p}{M_J} \right) \left(\frac{M_\odot}{M_*} \right)^{3/2} \left(\frac{a}{0.04 \text{ AU}} \right)^{9/2} \left(\frac{R_J}{R_p} \right)^3 \text{ Myr}, \quad (17)$$

$$\tau_e = \frac{e}{|de/dt|} = 0.33 \left(\frac{Q'_p}{10^6} \right) \left(\frac{M_p}{M_J} \right) \left(\frac{M_\odot}{M_*} \right)^{3/2} \left(\frac{a}{0.04 \text{ AU}} \right)^{13/2} \left(\frac{R_J}{R_p} \right)^5 \text{ Gyrs}. \quad (18)$$

The above derivation for τ_e is based on the approximations that the planet's spin is nearly synchronized with its mean motion and the tide raised on the planet by the star provides the dominant contribution to the e evolution. The magnitude of τ_e would be shortened/lengthened by the planet's tide raised on a slowly/rapidly (relative to Ω_{pc}) spinning star (DLM). From these equations we find

$$\tau_{\Omega p} = \frac{7\alpha_p\epsilon_p}{2} \left(\frac{R_p}{a} \right)^2 \left| \frac{\Omega_p}{\Omega_p - n} \right| \tau_e. \quad (19)$$

In the limits that $e \ll 1$ and $M_p \ll M_*$, $\tau_{\Omega p} \ll \tau_e$, and the nearly-synchronous approximation in equation (18) is justified self consistently.

Under the action of tidal torque and the conservation of total angular momentum, $\dot{J}_o = \dot{J}_p + \dot{J}_*$. In the case without mass transfer between the star and the planet, this exchange also leads to an evolution of the semi-major axis at a rate

$$\dot{a} = a \left(\frac{2e\dot{e}}{(1-e^2)} + \frac{2(\dot{J}_* + \dot{J}_p)}{J_o} - \frac{1}{\tau_d} \right) \quad (20)$$

where τ_d is the usual planetary migration time scale through disk-planet interaction. Since the planet quickly establishes a state of synchronous rotation, the magnitude of \dot{J}_p becomes much smaller than that of \dot{J}_* and $\tau_e = |e/\dot{e}| \ll \tau_{\Omega*} < |J_o/\dot{J}_*| < |J_o/\dot{J}_p|$ so that a declines together with e . But, after the orbit is circularized, a and $\dot{J}_* + \dot{J}_p$ evolve together with the same sign and the evolution of a is mainly driven by the dominant effect of the tide raised on the star by the planet (Goldreich & Soter 1966, Mardling & Lin 2002) such that

$$\tau_a \equiv \frac{a}{\dot{a}} \simeq \frac{Q'_* M_*}{9M_p} \frac{(a/R_*)^5}{(\Omega_* - n)} \simeq \left(\frac{7n}{\Omega_* - n} \right) \left(\frac{Q'_*}{10^6} \right) \left(\frac{M_*}{M_\odot} \right)^{1/2} \left(\frac{M_J}{M_p} \right) \left(\frac{a}{0.04 \text{ AU}} \right)^{13/2} \left(\frac{R_\odot}{R_*} \right)^5 \text{ Gyr} \quad (21)$$

in the limit $\tau_d = \infty$. Provided $Q'_* \sim Q'_p$ and $\beta \sim 1$, $\tau_a > \tau_e > \tau_\Omega$. For $R_* = R_\odot$, τ_a is much larger than τ_d (except for $a < 0.01 \text{ AU}$), and is also much larger than the relevant time scales τ_R and τ_e

for planetary inflation and eccentricity damping (which are ~ 1 Myr, see the discussions in §3.3, §5, and the simulation results in §6.2) that concern us in this paper. Thus, we can neglect the evolution of a due to the tide raised on the star by the planet today. But, during the classical T Tauri phase when $R_* \sim 3R_\odot$, Ω_* is a significant fraction of the breakup angular frequency, and $Q_* \sim 1.5 \times 10^5$, the magnitude of τ_a is comparable to that of τ_d ($\sim 10^{5-6}$ yr) at

$$a = a_{\text{halt}} \simeq \left(\frac{9M_p \tau_d \Omega_*}{Q_* M_*} \right)^{1/5} R_* \sim 0.03 - 0.04 \text{ AU} \quad (22)$$

such that protoplanets' migration induced by their tidal interaction with their protoplanetary disks may be stalled by that with their host stars (Lin et al. 1996). Although the magnitude of τ_d may differ from its assumed value of $\sim 10^5$ yr in the above estimate, a_{halt} has a very weak dependence on τ_d . The value of a_{halt} is also a weak function of Q'_* . Two orders of magnitude increase in Q'_* would reduce a_{halt} by a factor of < 3 .

3. Planet's Structural Adjustment due to its Internal Tidal Energy Dissipation

In this section, we consider 1) the effect of tidal dissipation in increasing the internal temperature of the planet, 2) the necessary conditions for planetary inflation, 3) the sufficient condition for Roche lobe overflow.

3.1. Energy budget

During the synchronization and circularization processes, kinetic energy is continually dissipated into heat. From equations (20) and (6) we find that both \dot{e} and $\dot{\Omega}_p$ lead to the evolution in a and a corresponding change in the orbital energy $E_{\text{orb}} = -GM_*M_p/2a$ at a rate

$$\dot{E}_{\text{orb}} = -E_{\text{orb}} \frac{\dot{a}}{a}. \quad (23)$$

In addition, the planet's spin energy $E_{\text{spin}} = I_p \Omega_p^2/2$ evolves at a rate

$$\dot{E}_{\text{spin}} = \dot{E}_{\text{spin}}^R + \dot{E}_{\text{spin}}^\Omega \equiv \alpha_p M_p R_p \dot{R}_p \Omega_p^2 + I_p \Omega_p \dot{\Omega}_p \quad (24)$$

where the first term on the right hand side represents the planet's size adjustment (see below), and the second term corresponds to the changes in the kinetic energy. From equations (6) and (20), we find

$$\dot{E}_{\text{tide}} \equiv \dot{E}_{\text{orb}} + \dot{E}_{\text{spin}}^\Omega = \mu n^2 a^2 \left(\frac{e\dot{e}}{1-e^2} \right) + I_p \Omega_p \dot{\Omega}_p = \mu (\dot{\mathbf{r}} - \mathbf{\Omega}_p \times \mathbf{r}) \cdot \mathbf{f}_t \quad (25)$$

is the total tidal energy dissipation rate within the planet in its rest frame (Eggleton et al. 1998, Mardling & Lin 2002). (A similar expression can be derived for the rate of energy dissipation

within the star, but its effect on the stellar structure is negligible.) From equations (5), (11), (12), and (25), we find

$$\dot{E}_{\text{tide}} = - \left(\frac{9\mu na^2}{2Q'_p} \right) \left(\frac{M_*}{M_p} \right) \left(\frac{R_p}{a} \right)^5 \left[\Omega_p^2 h_3(e) - 2n\Omega_p h_4(e) + n^2 h_5(e) \right], \quad (26)$$

where $h_3(e) = (1 + 3e^2 + 3e^4/8)(1 - e^2)^{-9/2}$, $h_4(e) = (1 + 15e^2/2 + 45e^4/8 + 5e^6/16)(1 - e^2)^{-6}$, and $h_5(e) = (1 + 31e^2/2 + 255e^4/8 + 185e^6/16 + 25e^8/64)(1 - e^2)^{-15/2}$.

For small e 's, the leading terms of e^2 and $\Omega_p/n - 1$ in equation (26) are reduced to

$$\dot{E}_{\text{tide}} = - \frac{9\mu a^2 n^3}{2Q'_p} \left(\frac{M_*}{M_p} \right) \left(\frac{R_p}{a} \right)^5 \left[\left(\frac{\Omega_p}{n} - 1 \right)^2 + e^2 \left(\frac{15\Omega_p^2}{2n^2} - \frac{27\Omega_p}{n} + 23 \right) \right] \quad (27)$$

The first term in the square bracket on the right hand side of the above equation represents the energy dissipation due to the synchronization of the planet's spin. If planets are formed as rapid rotators, similar to Jupiter and Saturn, equation (27) reduces to

$$\dot{E}_{\text{tide}} \simeq \dot{E}_{\text{t}\Omega} \equiv - \frac{I_p(\Omega_p - n)\Omega_p}{\tau_\Omega}. \quad (28)$$

When synchronization is established the terms inside the last bracket are reduced to $7e^2/2$ and equation (27) may be approximated as (c.f. Goldreich & Soter 1966)

$$\dot{E}_{\text{tide}} \simeq \dot{E}_{\text{te}} \equiv - \frac{e^2 GM_* M_p}{a\tau_e}. \quad (29)$$

We now consider the effect of tidal dissipation on the total energy budget of the system. In response to this source of energy, the planet adjusts its internal structure to evolve toward an energy equilibrium in which the rate of change of the planet's total energy is given by

$$\dot{E}_{\text{tot}} = \dot{E}_{\text{bind}} + \dot{E}_{\text{spin}} = -\mathcal{L} \quad (30)$$

where \mathcal{L} is the rate of loss of energy from the system via radiation from the planet's surface. In this derivation, we assume that the planet maintains a state of hydrostatic equilibrium. The tidal energy dissipation rate is contained in \dot{E}_{tot} in the following manner. The binding energy has three contributing components

$$E_{\text{bind}} = -q_* \frac{GM_*^2}{R_*(t)} - q_p \frac{GM_p^2}{R_p(t)} + E_{\text{orb}} \quad (31)$$

where $q_{*,p} = 3/(5 - n_{*,p})$ and $n_{*,p}$ is the polytropic index for the star and planet respectively. For a polytrope of index 1, $q_{*,p} = 3/4$ and for a uniform distribution of density, $q_{*,p} = 3/5$.

Neglecting any changes in the gravitational energy of the host star,

$$\dot{E}_{\text{bind}} = \frac{q_p GM_p^2}{R_p(t)} \frac{\dot{R}_p}{R_p} + \frac{GM_p M_*}{2a(t)} \frac{\dot{a}}{a}. \quad (32)$$

Note that M_p in the above equation can also be a function of time when the size of planet is inflated up to its Roche radius and therefore mass loss occurs. Similarly, the spin energy can be separated into two pieces (see eq. 24). In principle, rotation may also affect the binding energy of the planet. But from equations (31) and (24), we find the energy ratio

$$\frac{E_{\text{spin}}}{|E_{\text{bind}}|} = \frac{\alpha_p}{6q_p} \left(\frac{R_p}{R_L}\right)^3 \left(\frac{\Omega_p}{n}\right)^2 (1-e)^3 \quad (33)$$

where

$$R_L = \left(\frac{M_p}{3M_*}\right)^{1/3} a(1-e) \approx 5.74 \left(\frac{M_p}{M_J}\right)^{1/3} \left(\frac{M_\odot}{M_*}\right)^{1/3} \left(\frac{a}{0.04\text{AU}}\right) (1-e)R_J, \quad (34)$$

is the planet's Roche radius and M_J and R_J are Jupiter's mass and radius, respectively. After the planet attains synchronization within its Roche radius, its rotational energy is relatively small compared with its binding energy. Since $E_{\text{spin}} \ll E_{\text{bind}}$, the effects of Coriolis and centrifugal force are negligible in the calculation of the planet's internal structure. In the above expression for R_L , we introduce a factor of $(1-e)$ to represent the tidal radius at periastron where the stellar tidal effect is at an maximum.

3.2. Tidal inflation instability

Tidal dissipation within the planet leads to changes in a and Ω_p , and we have already defined the rate \dot{E}_{tide} in equation (25). This process also leads to the internal heating of the planet at a rate $-\dot{E}_{\text{tide}}$. From the above equations, we find that the planet's size would change at a rate

$$\dot{R}_p = \frac{-\mathcal{L} - \dot{E}_{\text{tide}}}{q_p G M_p^2 / R_p^2 + \alpha_p M_p R_p \Omega_p^2} \quad (35)$$

provided the adjustment would not directly modify α_p (Mardling & Lin 2002).

In a thermal equilibrium, $\dot{R}_p = 0$ and equation (35) reduces to

$$\mathcal{L} = \mathcal{L}_e \equiv -\dot{E}_{\text{tide}} \quad (36)$$

such that the surface radiative flux is balanced by internal energy dissipation. In response to a small perturbation δR_p from its equilibrium radius

$$R_e \equiv R_p(\mathcal{L} = -\dot{E}_{\text{tide}}) \quad (37)$$

and in the case of $\tau_e \gg \tau_R$ (*i.e.* e can be roughly treated as a constant with time for this small perturbation), a planet adjusts its radius at a rate

$$\dot{R}_p = \left(\frac{9\mu n a^2}{2Q'_p}\right) \left(\frac{M_*}{M_p}\right) \left(\frac{R_e}{a}\right)^5 \left(\frac{\Omega_p^2 h_3(e) - 2n\Omega_p h_4(e) + n^2 h_5(e)}{q_p G M_p^2 / R_p^2 + \alpha_p M_p R_p \Omega_p^2}\right) (5 - \gamma) \left(\frac{\delta R_p}{R_e}\right) \quad (38)$$

where

$$\gamma \equiv \left(\frac{\partial \ln \mathcal{L}}{\partial \ln R_p} \right)_{R_p=R_e} . \quad (39)$$

Note that \dot{R}_p and δR_p would have opposite signs and the thermal equilibrium would be stable if $\gamma > 5$. But if $\gamma < 5$, small increases in R_p would lead to runaway inflation.

In general \mathcal{L} is a function of M_p , R_p , and the existence of the core. Based on three sets of equilibrium models, BLM obtained an approximate $R_e - \mathcal{L}$ relations in which

$$\log \frac{R_e}{R_\odot} = A(M_p) + B(M_p) \log \frac{\mathcal{L}}{L_\odot} + C(M_p) \left(\log \frac{\mathcal{L}}{L_\odot} \right)^2 \quad (40)$$

where, in the range $10^{-8} L_\odot < \mathcal{L} < 10^{-5} L_\odot$, $A = (3.11, 1.012, -0.269)$, $B = (1.011, 0.4689, 0.1631)$, and $C = (0.0642, 0.0289, 0.00978)$ for $M_p = (0.63, 1, 8) M_J$ respectively. In the high luminosity limit, R_e becomes a more rapidly increasing function of \mathcal{L} (with a decreasing γ magnitude) as degeneracy and non-ideal effects in the equation of state are partially lifted for $R_p > 2R_J$. Based on the results of a limited number of models computed by BLM for $M_p = 0.63$ and $1M_J$ planets around HD 209458 and Ups And ¹, we find that γ crosses the critical value of 5 when $R_p = R_c \sim 2R_J$ in both cases and $\mathcal{L}_e = \mathcal{L}_c = (10^{-6}, 10^{-5.5} L_\odot)$ for $M_p = (0.63, 1M_J)$ respectively.

Although γ continues to decline for $R_p > R_c$, we introduce a power-law approximation

$$\frac{\mathcal{L}_e}{\mathcal{L}_o} \simeq \left(\frac{R_p}{2R_J} \right)^\gamma . \quad (41)$$

for a limited range of R_p . In the range of $R_p = 2 - 5R_J$, we fit the results of BLM with a normalization coefficient $\mathcal{L}_o = 10^{-6} L_\odot$ and $\gamma = 3$ for a $M_p = 0.63 M_J$ planet. This prescription is chosen for computational convenience and consistency, *i.e.* $\mathcal{L}_e = \mathcal{L}_c$ for $R_p = R_c \sim 2R_J$. In §5, we present additional numerical models which also indicate $\gamma < 5$ for $R_p > 2R_J$ for other values of M_p .

In this limit, the thermal equilibrium is linearly unstable to tidal dissipation. A small enlargement in the planet's size from R_e would cause tidal dissipation to increase more rapidly than the radiative losses on its surface. However, e decays in the meantime. The question of whether the planet's R_p would finally reach the Roche radius depends on the magnitude of e : there exists a threshold e beyond which the planet is able to be inflated to its Roche radius, meaning that this process relies on a nonlinear instability. Similarly, a small reduction in R_p from R_e would lead to rapid cooling, and the planet would contract until R_p is reduced to R_c . The characteristic

¹The semi-major axis of HD209458b is actually about 0.045 AU. The only difference modeled by BLM for giant planets located at different a is the degree of stellar irradiation. However, BLM show that inflation of giant planets due to stellar irradiation is negligible compared with tidal inflation. Therefore the estimate performed in the text section based upon replacing 0.045 AU by 0.04 AU should serve as a good approximation.

contraction time scale at $R_p = R_c$ is

$$\tau_c = \frac{q_p GM_p^2}{R_c \mathcal{L}_c} = 1.6 \times 10^8 q_p \left(\frac{10^{-6} L_\odot}{\mathcal{L}_c} \right) \left(\frac{2R_J}{R_p} \right) \left(\frac{M_p}{M_J} \right)^2 \text{ yr.} \quad (42)$$

3.3. Necessary and sufficient condition for runaway planetary inflation

The above criterion for tidal inflation instability ($\gamma < 5$) is applied to a state of thermal equilibrium. In general, the planets may not be in such an equilibrium, and during the evolution toward it, tidal dissipation may modify their orbital properties. Therefore, it is essential to identify 1) the sufficient kinematic properties which would enable planets to inflate before their eccentricity is damped out and 2) the necessary initial conditions which may lead to an equilibrium radius R_e which exceeds a critical radius $R_c (\sim 2R_J)$ for the onset of tidal inflation instability. In the determination of the stability criteria, we must take into account the dynamical evolution of the planets' orbits.

Prior to reaching an equilibrium value of R_e , the planet's radius R_p adjusts at a rate in accordance with equation (35). Since $E_{\text{spin}} < E_{\text{bind}}$, this equation implies that R_p inflates on a time scale

$$\tau_R = \frac{R_p}{\dot{R}_p} \simeq -\frac{q_p GM_p^2}{\dot{E}_{\text{tide}} R_p} \quad (43)$$

in the limit that the tidal heating greatly exceeds the radiative cooling.

Note that equation (35) is based on the implicit assumption that \dot{R}_p is uniquely determined by a given set of R_p , M_p , and \dot{E}_{tide} regardless of the thermal history of the planet's interior. In principle, the evolution of stratification of planets due to thermal imbalance in a state of quasi-hydrostatic equilibrium should be a function of the heating mechanism. But, gas inside Jupiter-mass giant planets is partially degenerate and non-ideal such that the total pressure is insensitive to temperature changes. BLM presented several models with different dissipation prescriptions. The results of all their models show that a large fraction of the energy dissipated within the planet leads to temperature increases without significantly modifying the pressure and thermal stratification of the convective interior of the planet. Only the tenuous radiative zone in the outermost 10% of the planet's radius responds to heating like an ideal gas. Thus, tidal dissipation only affects the boundary condition at the interface between the convective and radiative zones as well as the structure of the radiative zone, and our approximation is justified.

During the process of synchronization, although the total amount of energy available (E_{spin}) is limited, it is dissipated on a rapid time scale of τ_Ω such that $\dot{E}_{\text{tide}} \simeq \dot{E}_{\text{t}\Omega}$. From equations (28) and (43), we find

$$\tau_R \simeq \tau_{R\Omega} \simeq \frac{\Omega_{kp}^2 \tau_\Omega}{\Omega_p |\Omega_p - n|} \left(\frac{q_p}{\alpha_p} \right) \quad (44)$$

where Ω_{kp} is the breakup spin frequency of the planet, and $\tau_{R\Omega}$ is the planetary-inflation time scale in the limit where only the effect of synchronization is considered. Since $\Omega_p < \Omega_{kp}$ and α_p is relatively small, $\tau_{R\Omega} > \tau_\Omega$ and the planet does not have time to inflate in size before its spin become synchronized with its mean motion.

Energy is also dissipated within the planet during e damping. In order for a planet to be inflated by e damping against its own gravitational binding energy, e should decay on a longer time scale (τ_e) than the thermal time scale associated with inflation (τ_R); that is, the system should not run out of its dissipation energy source before it overflows its Roche radius. From equations(29) and (43), we find that, in the limit that tidal dissipation mainly leads to circularization,

$$\tau_R \simeq \tau_{Re} \simeq q_p \left(\frac{M_p}{M_*} \right) \left(\frac{a}{R_p} \right) \left(\frac{\tau_e}{\beta e^2} \right) \simeq 3q_p \left(\frac{R_L \tau_e}{R_p \beta} \right) \left(\frac{R_L}{ae} \right)^2 = \frac{e_R^2 \tau_e}{e^2}. \quad (45)$$

The necessary condition for planetary inflation ($\tau_R < \tau_e$) is satisfied in the limit that its e is greater than a critical value

$$e > e_R \simeq \left(\frac{q_p M_p a}{\beta M_* R_p} \right)^{1/2} = 0.18 \left(\frac{q_p M_p M_\odot 2R_J a}{0.75\beta M_J M_* R_p 0.04\text{AU}} \right)^{1/2}. \quad (46)$$

In the above expression, e_R decreases with R_p so that the most stringent requirement for a protoplanet to inflate is set prior to its expansion. If short-period planets migrated to their present location within a few Myr after their dynamical accretion of ambient gas in the protostellar disk has ceased, their initial R_p would be $\sim 2R_J$ (Pollack et al. 1996). In equation (46), we use a fiducial value of $2R_J$ for R_p which is also comparable to the value of R_c . During the same early epoch, main sequence G dwarf stars are rapid rotators and have relatively small Q'_* so that for relatively large R_p , β is slightly less than unity. Note that in equation (46) e_R is independent of Q'_p such that it is not subject to the uncertainties in the tidal dissipation rate.

Short-period planets with initial $e > e_R$ would inflate until they reached a thermal equilibrium with a radius $R_p = R_e$. Those planets with $e \gg e_R$ would retain their initial e as they approached the thermal equilibrium. But those planets with an initial e marginally larger than e_R would undergo a substantial e damping prior to reaching the thermal equilibrium. Thus, it is possible for some planets to initially satisfy the necessary condition for tidal inflation, and become stabilized after their e is substantially reduced. Thus, the instability criterion in equation (46) should be regarded in a qualitative sense.

Equation (37) indicates that R_e is a function of \dot{E}_{tide} . Assuming the planet has already attained spin-orbit synchronization (so that $\dot{E}_{\text{tide}} \sim \dot{E}_{\text{te}}$), we find from equations(18), (41), and (37) that

$$\frac{R_e}{R_s} = \left(\frac{e_L(R_s)}{e} \right)^{\frac{2}{5-\gamma}} \quad (47)$$

where R_s is a fiducial length scale and

$$\begin{aligned}
 e_L(R_s) &= \left(\frac{a\tau_e(R_e = R_s)\mathcal{L}_e(R_e = R_s)}{GM_*M_p} \right)^{1/2} \\
 &\simeq 0.056 \left(\frac{Q'_p}{10^6} \right)^{1/2} \left(\frac{M_\odot}{M_*} \right)^{5/4} \left(\frac{a}{0.04\text{AU}} \right)^{15/4} \left(\frac{\mathcal{L}_o}{10^{-6}L_\odot} \right)^{1/2} \left(\frac{2R_J}{R_s} \right)^{(5-\gamma)/2} \\
 &\simeq 0.06 \left(\frac{Q'_p}{10^6} \right)^{1/2} \left(\frac{P}{3\text{days}} \right)^{5/2} \left(\frac{\mathcal{L}_o}{10^{-6}L_\odot} \right)^{1/2} \left(\frac{2R_J}{R_s} \right)^{(5-\gamma)/2}
 \end{aligned} \tag{48}$$

where we adopt the approximation in equation (41) for \mathcal{L} and scale R_s with $2R_J$. Note that although M_p does not appear directly in equation (48), both e_L and \mathcal{L}_o are slowly increasing functions of M_p .

In the previous section, we showed that a planet would adjust to a stable equilibrium size if $R_e < R_c (\sim 2R_J)$. But, for $R_e > R_c$, $\gamma < 5$, and the planet is unstable such that it would undergo runaway inflation if its current size $R_p < R_e$ or contraction to R_s if $R_p > R_e$. In principle, we should set $R_s = R_p$ in equations (47) and (48). But, the critical e_L should not be a decreasing function of R_s as indicated in equation (48). For example, the Roche radius of a $0.63M_J$ planet, located at $a = 0.04\text{AU}$ around a $1.1 M_\odot$ star (HD 209458), is $R_L = 4.92R_J$. An extrapolation from Fig. 3 in BLM shows that an internal heating rate of at least $\approx 10^{-4.9} L_\odot$ is required for a coreless $M_p = 0.63M_J$ planet to attain $R_e = R_L$ in this case. Nevertheless, the critical eccentricity e_L for R_e to reach R_L is less than half that needed for R_e to reach $\sim 2R_J$ (*i.e.* $< 0.5e_L$) because the efficiency of tidal dissipation increases rapidly with R_p . Thus, analogous to the planet's R_p dependence in e_R , the most stringent requirement for a protoplanet to inflate is set prior to its expansion rather than the final post-inflation value of R_L . In the limit that the planet's initial radius $R_i < R_e$, the appropriate sufficient condition for the onset of runaway inflation is

$$e > e_L(R_s = R_c). \tag{49}$$

Once again, note that e may be damp during the course of the planet's size adjustment, especially for those systems with $e(R_i)$ marginally larger than $e_R(R_i)$. In these cases, the value of the e in the above expression should be $e(R_c)$ (see further discussions in §6).

The power-law approximation in equation (41) and its extrapolation in equation (48) are only appropriate for R_p in the range of $1 - 3R_c$ where $\gamma < 5$. In the limit $R_s = R_c$, $\gamma = 5$, $\mathcal{L}_e = \mathcal{L}_c$, and

$$\begin{aligned}
 e_L(R_s = R_c) &\simeq 0.056 \left(\frac{Q'_p}{10^6} \right)^{1/2} \left(\frac{M_\odot}{M_*} \right)^{5/4} \left(\frac{a}{0.04\text{AU}} \right)^{15/4} \left(\frac{\mathcal{L}_c}{10^{-6}L_\odot} \right)^{1/2} \\
 &\simeq 0.06 \left(\frac{Q'_p}{10^6} \right)^{1/2} \left(\frac{P}{3\text{days}} \right)^{5/2} \left(\frac{\mathcal{L}_c}{10^{-6}L_\odot} \right)^{1/2}.
 \end{aligned} \tag{50}$$

3.4. The onset of planets' inflation to their Roche lobes

If a planet migrated to the vicinity of its host star with an initial radius $R_i < R_c$ and with e larger than both e_L in equation (50) and e_R in equation (46), it would undergo runaway tidal inflation. For $a > a_{RL}$ where

$$a_{RL} = 0.06 \left(\frac{q_p/\beta}{0.75} \frac{10^6}{Q'_p} \frac{M_p}{M_J} \frac{10^{-6} L_\odot}{\mathcal{L}_o} \right)^{2/13} \left(\frac{M_*}{M_\odot} \right)^{3/13} \left(\frac{2R_J}{R_p} \right)^{\frac{2\gamma-8}{13}} \text{ AU}, \quad (51)$$

$e_R < e_L$ so that the condition for planetary inflation is $e > e_L$. But, a planet with $a < a_{RL}$, can only inflate if $e > e_R$. For a $M_p = 0.63M_J$ planet ($\gamma = 3$ and $\mathcal{L}_o = 10^{-6}L_\odot$), a_{RL} increases with R_p . Although it is possible for $e_L(R_c) > e_R(R_c)$ and $e_L(R_L) < e_R(R_L)$ at some locations, the runaway tidal inflation following the onset of the thermal instability always leads the planet to overflow its Roche lobe because both $e_L(R_c) > e_L(R_L)$ and $e_R(R_c) > e_R(R_L)$ such that the sufficient and necessary conditions for runaway inflation become more easily satisfied during the planet's expansion. Note that the magnitude of a_{RL} is very weakly dependent on that of Q'_p . Two orders of magnitude uncertainty in Q'_p would correspond to a factor of two difference in a_{RL} . Thus, our results are quite robust despite the uncertainties in the magnitude of Q'_p .

Equation (46) indicates that $e_R \propto a^{1/2}$ and it reduces to ~ 0.06 near the surface of a star. However, even in the limit that e is larger than both e_R and e_L , the planet's R_p is limited by R_L which is smaller than R_c if

$$a < a_c = 0.0133 \left(\frac{M_J}{M_p} \right)^{1/3} \left(\frac{M_*}{M_\odot} \right)^{1/3} \left(\frac{R_c}{2R_J} \right) \text{ AU}. \quad (52)$$

Inside a_c , planets cannot expand into the unstable range. Nevertheless, $R_e > R_c$ (and therefore R_L) for $e > e_L(R_c)$ which is very small at such close range (see eq. 48). In this limit, planets with $e > e_R$ (so their e -value may be maintained) would overflow their Roche radius for all values of β .

The metallicity of many planet-bearing stars is higher than the solar value. It has been suggested that the outer convective zone of some of these stars may be contaminated by the consumption of one or more planets which may have undergone orbital decay due to the star-planet tidal interaction (Lin 1997). Previous models for such a process focus on the disintegration of planets inside the envelope of their host stars (Sandquist et al. 1998, 2002). The present results suggest that with a modest e -value, short-period planets may be disrupted during their tidal orbital decay prior to entering the envelope of their host stars.

A planet with $a > a_{RL}$ and $R_i < R_c$ would undergo runaway inflation if $e > e_L(R_c)$. The expression in equation(50) also indicates that $e_L \propto a^{15/4}$ so that a planet would inflate and fill its Roche radius provided its initial a is less than a_{eL} where

$$a_{eL} = 0.086e^{4/15} \left(\frac{10^6}{Q'_p} \right)^{2/15} \left(\frac{R_c}{2R_J} \right)^{2/3} \left(\frac{10^{-6}L_\odot}{\mathcal{L}_c} \right)^{2/15} \text{ AU} \quad (53)$$

or initial P is less than P_{eL} where

$$P_{eL} = 9.24e^{4/15} \left(\frac{10^6}{Q'_p} \right)^{1/5} \left(\frac{R_c}{2R_J} \right) \left(\frac{10^{-6}L_\odot}{\mathcal{L}_c} \right)^{1/5} \text{ days.} \quad (54)$$

Over the possible range of Jupiter's Q-value $5 \times 10^4 < Q'_p < 2 \times 10^6$, $R_c (\simeq 2R_J)$, and $\mathcal{L}_c (\simeq 10^{-6}L_\odot$ for the $M_p = 0.63M_\odot$ planet), tidal inflation from $R_i < R_c$ to Roche lobe overflow becomes unattainable for $a > 0.08 - 0.13$ AU or $P > 8 - 17$ days. For these values of a , M_p , R_c , and $\beta \sim 1$, equations (18) and (43) imply $\tau_R \sim \tau_e < a$ few Myrs.

It is possible, though less likely, that protoplanets may be brought to the vicinity of their stars while they are still in the accretion phase so that their initial R_i is larger than R_c . In this case, the planets are already in a thermally unstable region. These planets would undergo runaway inflation if their $R_e > R_i$ and contraction to R_c if their $R_e < R_i$. A direct comparison between R_e and R_i can be made with equations (47) and (48) by setting $R_s = R_i$ such that

$$\frac{R_e}{R_i} = \left(\frac{e_L(R_i)}{e} \right)^{\frac{2}{5-\gamma}} \quad (55)$$

where

$$e_L(R_i) = \left(\frac{R_c}{R_i} \right)^{(5-\gamma)/2} e_L(R_c) < e_L(R_c). \quad (56)$$

For $a > a_{RL}$, runaway inflation from $R_i (> R_c)$ would occur if $e > e_L(R_i)$.

In the above derivation of e_L , we explicitly assumed that the planet's spin is nearly synchronized with its orbit. Equation (27) clearly shows that a significant departure from the $\Omega = n$ synchronization state would lead to an additional source of tidal dissipation of energy. During its inflation, the planet's spin frequency would decrease with a rate $\dot{\Omega}_{pc} = -2\Omega_p \dot{R}_p / R_p = -2\Omega_p / \tau_R$ if its spin angular momentum is conserved. Nevertheless, quasi-synchronization would be maintained if $\dot{\Omega}_{pc}$ is balanced by the tidally induced $\dot{\Omega}_p$ in equation (9), *i.e.*

$$\tau_\Omega \sim \tau_R / 2. \quad (57)$$

Under the assumption that most of the energy is dissipated through circularization (an assumption to be satisfied self consistently below), equations (19), (45), and (57) imply that the planet's spin attains an equilibrium with

$$\frac{\Omega_p - n}{\Omega_p} \simeq \frac{14e^2}{3q_p} \left(\frac{R_p}{R_L} \right)^3. \quad (58)$$

With such a small departure of Ω_p from n , energy dissipation associated with the circularization process continues to provide the dominant heat source as shown in equation (27).

3.5. Planets' initial eccentricity

Extrasolar planets with $a \gtrsim 0.1$ AU have a nearly uniform e distribution between 0-0.7. All of the dozen extrasolar planets with period between 3-7 days and most planets with $a \lesssim 0.1$ AU

have negligible e 's. This dichotomy is probably due to the tidal circularization of short-period planets' orbits during the main sequence life span of their host stars. All the observed short-period planets have $a > 0.04\text{AU}$. Although some of these planets may have undergone tidal inflation if their initial $e > e_r$ (see eq. 46), but outside $\sim 0.08 - 0.13 \text{ AU}$, e_L rapidly increases above unity (see eq. 48) so that the rate of tidal dissipation is so weak that the planets' thermal equilibrium size is always less than their Roche radius.

Interior to 0.04 AU , however, a planet would be inflated to overflow its Roche radius provided $\tau_r < \tau_e$ or equivalently $e > e_r$ which is < 0.18 (see eq. 46). We note that if the extrasolar planets with $a \gtrsim 0.1 \text{ AU}$ retain their *ab initio* e distribution, most planets, including those with $a < 0.04\text{AU}$, would have initial $e > e_r$.

In addition to the extrapolation of the e distribution from the long-period planets, there are several theoretical reasons to expect the initial e of short-period planets to be much larger than their present values. These short-period planets are most likely to have formed at much larger distances from their host stars. Long-term dynamical instability may induce the mature planets to undergo close encounters with each other, causing some planets to be scattered to the close proximity of their host stars with large e 's (Rasio & Ford 1996, Ford 1996, Weidenschilling & Marzari 1996, Lin & Ida 1997). In comparison with the value of e_r , these planets would satisfy the necessary criterion for inflation when their a is reduced (along with their e) by the circularization process (Rasio et al. 1997) to a magnitude $< 0.04\text{AU}$.

Short-period planets may also have been brought to the proximity of their host stars during their formation stage as a consequence of the planet-disk tidal interaction (Lin et al. 1996) through wave excitation at the planets' corotation and Lindblad resonances. Energy and angular momentum transfers via the planets' corotation resonances damp their e 's whereas those through their Lindblad resonances excite their e 's (Goldreich & Tremaine 1980). Both processes induce gap formation in the disk near the planets' orbit. Massive planets with $M_p > 0.01M_*$ clear a wide gap such that regions containing all the corotation resonances are void of gas. The interaction between the disk gas and these massive planets through the Lindblad resonances excites e to several times the aspect ratio of the disk (Artymowicz 1992, Papaloizou et al. 2001, Goldreich & Sari 2002) which is typically $> e_r$.

In contrast, modest-mass planets with $M_p < 0.01M_*$ open narrow gaps, and residual disk gas may still occupy their corotation resonances close to their orbits. The dominance of the corotation over the Lindblad resonances induces e damping to negligible values. However, short-period protoplanets' e 's may also be excited by the processes which halted their orbital migration. For example, some young stellar objects are observed to have strong magnetic fields (Johns-Krull et al. 1999) and their magnetospheres may clear an inner cavity in their surrounding protostellar disks (Konigl 1991; Shu et al. 1994). As they enter into the cavity and retreat inwards from the disk's inner edge, the planets' corotation resonances evolve into the tenuous regions prior to their more distant Lindblad resonances. Thus, during the decline of the planet-disk tidal interaction, the

e -damping process diminishes more rapidly than the e -excitation process. Eventually, the planets' inward migration is terminated when all of their lowest-order Lindblad resonances have retreated into the cavity. But, during the transition stage, the planets' e 's may grow to be comparable to the fractional difference between the corotation and Lindblad resonances which is $\gtrsim e_r$ inside 0.04 AU.

Planets' migration may also be stalled if their loss of angular momentum to the disk is compensated by a transfer of angular momentum from the spin of their rapidly rotating host stars through their mutual tidal interaction. This process is effective in the limit that a is sufficiently small ($< a_{\text{halt}}$) for the stellar tidal force to be intense and that the stellar spin frequency $\Omega_* > n$ (see eq. 22). Fast Ω_* are observed among young stellar objects, with some reaching the stellar breakup values (Stassun et al. 1999). In equation (13), the star's contribution to \dot{e} is neglected. However, the stellar tidal effect would excite the planets' e if $\beta < 0$ or equivalently,

$$\Omega_* > \left[\frac{7}{11} \left(\frac{Q'_*}{Q'_p} \right) \left(\frac{M_*}{M_p} \right)^2 \left(\frac{R_p}{R_*} \right)^5 + \frac{18}{11} \right] n \quad (59)$$

which $\simeq 8n$ in the limit that $Q'_s = Q'_p$ and the average density of the planet equal to that of the star (DLM).

Another mechanism to stop planets' migration is through the rapid depletion of the disk which would quench their tidal interaction. Signs for additional planets are found around more than half of all the host stars with known planets. The e 's of multiple planets around the same host star are modulated as they exchange angular momentum through secular interaction. During the depletion of the disk, the procession frequencies of the planets also evolve with the gravitational potential of the depleting disk. This evolution leads to a sweeping secular resonance (Ward 1981) which may also induce the excitation of eccentricity for some planets (Nagasawa et al. 2002).

4. Mass Loss from Inflated Planets

Planets with $e > e_r$ inflate before their orbits are circularized. If their $e > e_L$, the expansion of their envelope would continue until it reached the Roche radius. In this section, we consider the flow pattern associated with the mass loss process.

4.1. Density scale height near the Roche lobe

In a quasi-hydrostatic equilibrium, the planet's surface is determined by the equipotential surfaces. For planets with circular orbits, the dimensionless potential in a frame which co-rotates with their mean motion is reduced to

$$U = \left(1 - \frac{M_p}{M_t} \right) \left(\frac{1}{r_1} + \frac{r_1^2}{2} \right) + \frac{M_p}{M_t} \left(\frac{1}{r_2} + \frac{r_2^2}{2} \right) \quad (60)$$

where r_1 and r_2 are the dimensionless distances from the host star and the planet, respectively (Murray & Dermott 1999). The physical values of r_1 and r_2 are obtained by multiplying them by a , and that of U can be obtained by multiplying it by GM_t/a .

For this potential, there are two locations, L1 and L2, near the planet which are saddle points. Both points lie on the line joining the planet and the host star, with L1 between them and L2 farther away from the host star than the planet. The distances of the L1 and L2 points (D_{L1} and D_{L2}) to the center of the planet are

$$D_{L1,L2} \simeq \left[\alpha \mp \frac{\alpha^2}{3} \right] a \quad (61)$$

where $\alpha \equiv (M_p/3M_*)^{1/3}$. Gas that expands beyond the L1 point falls toward and is accreted by the host star, whereas that which expands beyond the L2 point spirals outwards to form an excretion disk.

The equipotential surfaces containing L1 or L2 points are distorted from spherical symmetry about the planet. On the planet’s “night side” (in the direction of L2), the distance between the planet’s center and the closest point (L1’) on the equipotential surface which contains the L1 point is

$$D'_{L1} \simeq D_{L1} - \frac{2}{3}\alpha^{3/2}a. \quad (62)$$

The distance between the L1’ and the L2 points is

$$\Delta D = D_{L2} - D'_{L1} \simeq \frac{2a}{3}(\alpha^{3/2} + \alpha^2) \quad (63)$$

which for a Jupiter-mass planet is of the order of a few percent of D_{L1} . It is possible for the planet’s envelope to reach the equipotential surface containing the L1 point but not that containing the L2 point.

However, it is also possible for both equipotential surfaces to be contained within the planet’s atmosphere. For an isothermal planetary atmosphere, the density (ρ) scale height

$$h_\rho = \frac{\rho}{(\partial\rho/\partial r)} = \frac{c_s^2(r_p)}{\nabla\Psi}. \quad (64)$$

The gradient of the potential near the L1’ point is

$$\nabla\Psi = -\frac{GM_t}{a^2} \frac{dU}{dr_2} \simeq 4\alpha^{3/2} \frac{GM_t}{a^2} \quad (65)$$

which is somewhat softer than that of isolated planets. The ratio

$$\frac{h_\rho}{\Delta D} \simeq \frac{9}{8} \frac{\mathcal{R}_g T_p a}{\mu_g GM_p} \quad (66)$$

where T_p and $c_s(r_p)$ are, respectively, the temperature and sound speed of the planetary surface, and \mathcal{R}_g and μ_g are the gas constant and molecular weight. On their day side, planets are heated

to an equilibrium temperature $T_p \sim T_*(R_*/a)^{1/2}$, where the surface temperature of solar-type host stars is $T_* \sim 6 \times 10^3$ K. For Jupiter-mass planets at ~ 0.04 AU, $h_\rho \sim \Delta D$, such that both L1 and L2 may be contained in their atmosphere as the envelope fills the Roche radius.

In the above estimate, we used the day-side equilibrium temperature to estimate T_p . But both L1' and L2 points are on the “night-side” of the planet and are shielded from the stellar radiation. In principle, the night side of a mature planet could have a substantially lower surface temperature if the cooling time scale there is much shorter than the time scale for sound waves to cross the dark hemisphere. But, the resulting longitudinal pressure gradient would excite large scale circulation with speeds comparable to c_s of the hot side (Showman & Guillot 2002, Burkert et al. 2002); it is not clear yet what the resulting temperature on the dark side would be. For planets with relatively young ages ($t_p \approx 10^6 - 10^7$ yr), however, the effective temperature of unheated Jupiter-mass planets arising from their intrinsic luminosity (Burrows et al. 1997) falls in the range 500 – 800 K. If the planets migrated too close to their host stars and became tidally inflated shortly after they were formed, the stellar heating would introduce little temperature difference between the day and night sides of the planet.

In addition, if there is sufficiently intense energy dissipation in some planets to inflate their R_p beyond their R_L , their surface luminosity $\mathcal{L}_c(R_L)$ would exceed $10^{-5}L_\odot$ (see §3.2). For these tidally inflated planets with $R_p \sim R_L > 2R_J$, equations (40) and (41) are the more appropriate approximations. Using a black body scaling law $\mathcal{L}/L_\odot = (R_p/R_\odot)^2(T_p/T_\odot)^4$ where $T_\odot = 5800$ K is the effective temperature of the Sun and equation (41), we find that when $R_p = R_L$,

$$T_p \simeq T_\odot \left(\frac{\mathcal{L}}{L_\odot} \right)^{1/4} \left(\frac{R_L}{2R_J} \right)^{\gamma/4-1/2} \left(\frac{R_\odot}{2R_J} \right)^{1/2} \quad (67)$$

which for a $M_p = 0.63M_J$ planet is $\sim 700 - 1000$ K. In this limit, h_ρ may be a fraction of ΔD . But, we also note that near both the L1 and L2 points, the magnitude of $\nabla\Psi$ vanishes so that h_ρ may be substantially larger than that in equation (66) for the L1' point.

4.2. Mass flow induced by envelope expansion

We consider the flow across equipotential surfaces below but near the L1 point. For computational convenience, we adopt a spherically symmetric approximation for the equipotential surface. During the quasi-static expansion of the envelope, the mass flux advected from the planet’s interior across U is

$$\dot{M}_a(U) \simeq 4\pi\rho(U)r^2(U)V_r(U) \quad (68)$$

where $V_r(U)$ is the outflow speed across the equipotential surface located at a radius $r(U)$ from the planet’s center. V_r should not be confused with the size expansion rate \dot{R}_p . Assuming the planet’s expansion is homogeneous, we can approximate

$$\frac{\dot{M}_a(U)}{M_p} \simeq \lambda \frac{\dot{R}_p}{R_p} = \frac{\lambda}{\tau_R} \quad (69)$$

where λ is a positive dimensionless structure parameter. We show below that for a homogeneous interior, $\lambda = 3$ and it is of the same order but slightly less than 3 for more realistic models.

Neglecting departure from spherical symmetry, we define the equipotential surface U to be located at a distance $R_L(t)$ from the planet's center. At any given time t_1 , the mass interior to R_L is $M_\delta(t_1) = 4\pi \int_0^{R_L(t_1)} \rho(r, t_1) r^2 dr$. For $R_p > R_L$, the mass outside R_L , *i.e.* that between R_L and R_p , would be lost. At a later time $t_2 = t_1 + \Delta t$, the planet's density distribution, size, and Roche radius evolve at rates $\dot{\rho}$, \dot{R}_p , and \dot{R}_L respectively. The difference in the mass contained in R_L becomes

$$\dot{M}_\delta(t_1) = \frac{\Delta M_\delta(t_1)}{\Delta t} = \left(\frac{M_\delta(t_2) - M_\delta(t_1)}{\Delta t} \right) \simeq 4\pi \rho(R_L(t_1)) R_L(t_1)^2 \dot{R}_L + 4\pi \int_0^{R_L(t_1)} \dot{\rho} r^2 dr. \quad (70)$$

In a Roche potential,

$$\frac{\dot{R}_L}{R_L} = \frac{1}{3} \left(\frac{\dot{M}_\delta(t_1)}{4\pi \int_0^{R_L(t_1)} \rho r^2 dr} \right). \quad (71)$$

From equations (70) and (71), we find

$$\dot{M}_\delta(t_1) \left(1 - \frac{\rho(R_1, t_1) R_L(t_1)^3}{3 \int_0^{R_L(t_1)} \rho r^2 dr} \right) = 4\pi \int_0^{R_L(t_1)} \dot{\rho} r^2 dr. \quad (72)$$

In the limit that R_p is slightly larger than R_L , mass loss occurs near the atmosphere where the density is low and the second term on the left hand side of equation (72) is very small. But, after the planet's atmosphere is removed, the envelope continues to expand. The atmosphere merely responds with an expansion to restore a state of hydrostatic equilibrium. The actual value for $\rho(R_1, t_1)$ is that prior to the removal of the envelope between R_L and R_p .

An approximate solution can be constructed in which we consider the limit that R_L is much smaller than the original R_p . We first consider the rate of change of density in terms of the rate of change of some intermediate reference radius \dot{R}_r . The results of numerical models of planetary interiors (see §5) indicate that the inflation is nearly homologous, *i.e.* the ratio of the half density radius changes as $R_{1/2} \propto R_p^{\zeta_1}$ where $\zeta_1 \simeq 0.47$. The central density $\rho_c \propto R_p^{\zeta_2}$ where $\zeta_2 \simeq -1.35$. These numerical results also indicate that the density within $R_{1/2}$ is nearly homogeneous such that the mass contained within it $\sim 4\pi \rho_c R_{1/2}^3 / 3$ is approximately constant.

In order to derive the rate of change in density $\dot{\rho}$, we first consider a reference radius R_r which, at some time t_1 , contains a mass $\int_0^{R_r(t_1)} \rho(t_1) r^2 dr = M_r$. At $t_2 = t_1 + \Delta t$, the radius which contains the same amount of mass has evolved to $R_r + \dot{R}_r \Delta t$ while the density evolves at a rate $\dot{\rho}$ so that $\int_0^{R_r(t_1) + \dot{R}_r(t_1) \Delta t} (\rho(t_1) + \dot{\rho}(t_1) \Delta t) r^2 dr = M_r$. Note that although M_p may decrease due to mass loss, but, M_r is chosen to attain the same value. From these expressions of M_r , we find

$$\int_0^{R_r(t_1)} \dot{\rho}(t_1) r^2 dr = -\rho(R_r, t_1) R_r(t_1)^3 \frac{\dot{R}_r(t_1)}{R_r(t_1)}. \quad (73)$$

Note that the rate of change \dot{R}_r includes that due to tidal dissipation as well as mass loss. For isolated planets with $M_p > M_J$, $\partial R_p / \partial M_p < 0$ because the planet's interior is in a partially degenerate state. Thus, mass loss may also lead to size increases.

Without the loss of generality, we can choose R_r to be R_L in the above expression so that we find from equations(72) and (73) that

$$\frac{\dot{M}_\delta(t_1)}{M_p} \left(1 - \frac{4\pi\rho(R_L)R_L^3}{3M_p} \right) \simeq \frac{4\pi\rho(R_L)R_L^3}{M_p} \left(\frac{\dot{R}_r}{R_r} \right)_{R_L}. \quad (74)$$

Setting $\dot{M}_\delta = \dot{M}_a$, we find from eqs (74) and (69) that

$$\lambda \sim \frac{4\pi\rho(R_L)R_L^3}{M_p} \frac{(\dot{R}_r/R_r)_{R_L}}{\dot{R}_p/R_p}. \quad (75)$$

Shortly after overflowing the Roche radius R_L , $(\dot{R}_r/R_r)_{R_L} \simeq \dot{R}_p/R_p$ and $\rho(R_L)$ is very small. But in the advanced stage of Roche lobe overflow, $(\dot{R}_r/R_r)_{R_L} \simeq \dot{R}_{1/2}/R_{1/2} \simeq \zeta_1 \dot{R}_p/R_p$ but $\rho(R_L)$ may be only slightly smaller than ρ_c . For a nearly homogeneous planetary interior $\lambda \sim 3$ and if it is more central condensed, $\lambda < 3$. Our numerical models for their interior indicate that under the heating due to the tidal dissipation, planets establish a quasi hydrostatic equilibrium prior to reaching a thermal equilibrium. Since most of the gaseous giant planets' interior is convective, the temperature gradient is essentially adiabatic and the average global adiabatic index is ~ 1 . In these models, λ is of the same order but slightly less than 3. The numerical results to be presented in §5 do not depend sensitively on the actual value of λ .

4.3. Mass flux through the L1 & L2 points

As the planet's envelope expands and fills its Roche lobe, gas in its atmosphere encounters and flows through the saddle-shape nozzle in the equipotential surface. Near this region, the above approximation based on spherical symmetry can no longer be applied. Instead, we consider a cylindrical geometry with an axis of symmetry along the line joining the planet and its host star. The planet's mass loss rate through the L1 point between the equipotential surface which contains it and that with an arbitrary value U_n is

$$\dot{M}_{L1}(U_n) \simeq \int_{U_1}^{U_n} \rho(U)c_s(U) \frac{d\sigma}{dU} dU \quad (76)$$

where σ is the cross section of the nozzle (Lubow & Shu 1975, Pringle 1985). Note that the total mass flux can be obtained by setting $U_n = U_\infty$. In a coordinate system in which x is defined to be the direction joining the centers of the planet and its host star, y is orthogonal to x and in the orbital plane, and z is orthogonal to both x and y , the narrowest opening of the nozzle occurs at $x \simeq x_{L1}$, with $\sigma = \pi(sa)^2$ lies in the $y - z$ plane perpendicular to the x axis and sa is the radius

of the nozzle. The dimensionless variable s is a function of U and it vanishes for $U(r < D_{L1})$. In the neighborhood of L1, $\partial U/\partial s \simeq 3s$ so that

$$\frac{d\sigma}{dU} = \frac{2\pi a^2 s}{(dU/ds)} \simeq \frac{2\pi a^2}{3}. \quad (77)$$

For the same region, we find from equation (64) that

$$\rho(s) = \rho_1 \exp\left(-\frac{3GM_t s^2}{2ac_s^2}\right) \quad (78)$$

where ρ_1 is the density at the L1 surface, and from equation (76), we find

$$\dot{M}_{L1}(s_n) = \frac{2\pi\rho_1 a^3 c_s^3}{3GM_t} \left[1 - \exp\left(-\frac{3GM_t s_n^2}{2ac_s^2}\right)\right] \quad (79)$$

where $s_n = [2(U_n - U_1)/3]^{1/2}$.

The expansion of the planet's envelope would continue so long as $\dot{M}_a(U) > \dot{M}_{L1}$. As the planet's envelope climbs out of the potential well, ρ would increase which leads to enhanced spillage via the L1 point. We now estimate the critical condition which may lead to Roche lobe overflow via the L2 point. The difference in the potential between L1 and L2 points is

$$\Delta U \simeq 2\alpha^3 \quad (80)$$

so that $s_{L2} = 2(M_p/M_*)^{1/2}/3$ and

$$\dot{M}_{L1}(s_{L2}) = \frac{2\pi\rho_1 a^3 c_s^3}{3GM_t} \left[1 - \exp\left(-\frac{2GM_p}{3ac_s^2}\right)\right] \quad (81)$$

The expansion of the envelope would terminate if a mass transfer equilibrium can be established in which

$$\dot{M}_{L1} = -\dot{M}_a(U(L1)) \quad (82)$$

if we neglect the adjustment of the equipotential surface due to mass loss and orbital evolution (for further discussions, see next subsection).

From equations (69), (81), and (82), we find that the mass transfer equilibrium via the L1 point would only be attainable if the local density

$$\rho(L1) \gtrsim \rho_c = \left(\frac{2\lambda}{3}\right) \left(\frac{\dot{R}_p}{c_s(L1)}\right) \left(\frac{GM_p}{R_p c_s^2}\right) \rho_a \quad (83)$$

where the planet's average density within its Roche lobe $\rho_a = 3M_p/4\pi R_L^3 \simeq 10^{-2} \text{g cm}^{-3}$ for a Jupiter mass planet at 0.04 AU. Since the envelope of the inflated planet expands at a speed $\dot{R}_p \ll c_s$, $\rho(L1) \ll \rho_a$. For $R_p = R_L$ and $e \sim 0.14$, equations (43) and (83) lead to

$$\rho_c \sim \frac{7\lambda\beta e^2}{6q_p Q'_p} \left(\frac{GM_p}{c_s^2 R_L}\right) \left(\frac{R_L n}{c_s}\right) \rho_a \sim 10^{-6} \rho_a \sim 10^{-8} \text{g cm}^{-3}. \quad (84)$$

Since $\rho_a \propto a^{-3}$, $c_s \propto a^{-1/4}$, and $n \propto a^{-3/2}$, ρ_c is proportional to $a^{-15/4}e^2$ and it would exceed 10^{-7}g cm^{-1} at $a < 0.025\text{AU}$, which corresponds to a 1.5 day period around a $1 M_\odot$ G dwarf.

When planets overflow their Roche radius, $\rho(L1)$ is comparable to the density ρ_{atm} at their effective radius where the optical depth is of the order unity. Although $\nabla\Psi = 0$ at the L1 point, it is $\sim GM_p/R_L^2$ or that given in equation (65) elsewhere on the equipotential surface which contains that point. At $a = 0.04$ AU where the day-side temperature of $T_p \sim 1 - 2 \times 10^3\text{K}$, we find from equation (64) that $h_\rho \sim 2 - 3 \times 10^9$ cm for a Jupiter-mass planet. For this T_p , the opacity of the atmospheric gas is $\kappa \sim 10^{-1} \text{cm}^2 \text{g}^{-1}$ so that $\rho_{atm} \sim 10^{-8}\text{g cm}^{-3}$. For modest e values and $a > 0.04$ AU, $\rho_{atm} > \rho_c$ such that the optically thin atmosphere engulfs both the L1 and L2 points. In this limit, the density at the L2 point can be derived from equations (64) and (80) to be

$$\rho_2 = \rho_1 \exp\left(-\frac{2GM_p}{3ac_s^2}\right). \quad (85)$$

On a $M_p = 1M_J$ planet at 0.04 AU from a G dwarf where $T_s \sim 10^3\text{K}$, $\rho_2 \sim 0.2\rho_1$ so that gas near the Roche lobe mostly flows toward the host star via the L1 point.

From equation (84) we find $\rho_c > \rho_{atm}$ for planets with

$$a < a_{L2} = \left[\left(\frac{3\rho_*}{\rho_{atm}}\right) \left(\frac{GM_p}{c_*^2 R_*}\right) \left(\frac{7\lambda\beta}{6q_p Q'_*}\right) \left(\frac{R_* n_*}{c_*}\right) e^2 \right]^{4/15} R_* \quad (86)$$

where $\rho_* = 3M_*/4\pi R_*^3$, $n_* = (GM_*/R_*^3)^{1/2}$, and $c_* = (\mathcal{R}_g T_*/\mu_g)^{1/2}$. For $e \sim e_R \sim 0.14$, $a_{L2} \simeq 0.03\text{AU}$. Equivalently, with a given a , $\rho_c > \rho_{atm}$ for planets with

$$e > e_{L2} = \left[\left(\frac{\rho_{atm}}{3\rho_*}\right) \left(\frac{c_*^2 R_*}{GM_p}\right) \left(\frac{6q_p Q'_*}{7\lambda\beta}\right) \left(\frac{c_*}{R_* n_*}\right) \left(\frac{a}{R_*}\right)^{15/4} \right]^{1/2}. \quad (87)$$

At $a = 0.03$ AU, $e_{L2} \simeq 0.14$. In this limit, the opaque regions of the envelope extend above the equipotential surface which contains the L1 point. The temperature and density scale height in the envelope are greater than their surface values so that the density differential between the L1 and L2 points is reduced. Consequently, gas at the planets' effective radius may flow through both L1 or L2 points with comparable rates. An accurate determination of the ratio of the mass flux and the specific angular momentum flux through the L1 and L2 points needs to be analyzed with more detailed numerical hydrodynamic simulations (Burkert & Lin 2003).

In §3, we showed that the necessary and sufficient criteria for planetary inflation are $e > e_r$ and $e > e_L$. The instantaneous tidal radius of eccentric planets may modulate by a fraction e . At the periastron, gas outside the planet's minimum tidal radius is removed. During other phases, the planet's atmosphere is refilled as it adjusts, on its internal dynamical time scale, to an evolving quasi hydrostatic equilibrium, while the underlying envelope re-expands on a much longer internal heating time scale. If the ratio

$$\frac{h_\rho}{2eD_{L1}} \simeq \frac{(3\alpha)^{1/2} \mathcal{R}_g T_p a}{4e \mu_g GM_p} \quad (88)$$

is comparable to or larger than unity, the planet’s atmosphere would overflow the Roche lobe at all orbital phases and the mass loss would be continuous. Otherwise, bursts of mass loss would occur during each periastron passage.

4.4. The rate of planets’ mass overflow through their Roche lobe

Planets’ Roche lobe overflow also leads to their orbital migration. If the overflow occurs through both L1 and L2 points, angular momentum exchange between the infalling and outflowing transferred gas would result in orbital migration. In general, mass loss would lead to a reduction in the Roche radius at a rate

$$\frac{\dot{R}_L}{R_L} = \left(\frac{(\dot{M}_{L1} + \dot{M}_{L2})}{3M_p} + \frac{\dot{a}}{a} - \frac{\dot{e}}{1-e} \right) \quad (89)$$

along with the equipotential surfaces which contain the L1 and L2 points. The shrinkage of the Roche lobe would enhance mass flux across the equipotential surfaces which contain both the L1 and L2 points by an amount

$$\frac{\dot{M}_R}{M_p} \simeq -\lambda \frac{\dot{R}_L}{R_L} \quad (90)$$

such that the effective mass flux across the equipotential surface of the newly adjusted Roche lobe $U'(L1)$ is

$$\dot{M}_e(U'(L1)) = \dot{M}_a(U(L1)) + \dot{M}_R. \quad (91)$$

In a mass transfer equilibrium, this mass flux is lost through the L1 and L2 points such that

$$(\dot{M}_{L1} + \dot{M}_{L2}) = -\dot{M}_e(U'(L1)). \quad (92)$$

For $e > e_{L2}$, mass is lost via both the L1 and L2 points. In this limit with the simplified assumption $\dot{a} \simeq 0$ ², we find, from equations(69), (89), (90), (91), and (92), the planets’ mass loss rate to be

$$\dot{M}_{L2} = - \left(\frac{\lambda M_p}{1 - \lambda/3} \right) \left(\frac{\dot{R}_p}{R_p} + \frac{\dot{e}}{(1-e)} \right). \quad (93)$$

For planets with a relatively flat density distribution (*i.e.* λ is smaller but close to 3), the magnitude of \dot{M}_{L1} can greatly exceed that of $\dot{M}_a(U(L1))$.

The reduction of the planet’s mass reduces the radial velocity amplitude K for Earth-based observers which is determined by

$$K = \frac{M_p \sin i}{M_t} \left(\frac{2\pi G(M_t)}{P} \right)^{1/3} (1 - e^2)^{-1/2}$$

²This over-simplified assumption is just for the demonstration of this possible scenario, and will be used in the next section. What exactly happens to a in this limit is undetermined in this paper as stated in the preceding section

$$\approx 1.41 \left(\frac{M_p \sin i}{0.01 M_J} \right) \left(\frac{M_\odot}{M_*} \right)^{2/3} \left(\frac{3 \text{ days}}{P} \right)^{1/3} (1 - e^2)^{-1/2} \text{ ms}^{-1}, \quad (94)$$

where P is the planet's period and i is the inclination angle of the orbit with respect to the line of sight. For an observational limit of 1 m s^{-1} , planets with a few Earth masses and $P \lesssim 3$ days would be undetectable with the Doppler method. Thus, a substantial mass loss may account for the absence of any extrasolar planets with $a \lesssim 0.04 \text{ AU}$.

If, however, $e < e_{L2}$, planets would overflow their Roche lobes mostly via the L1 point and they would move outwards as they absorb the angular momentum and energy from the transferred gas which flows toward their host stars. This dynamical property is analogous to conservative mass transfer from a low-mass to a high-mass star in an interacting binary system. Assuming all the transferred material is accreted by the host stars and the total angular momentum of the system is conserved, the semi-major axes of these planets would expand at a rate

$$\frac{\dot{a}_m}{a} = 2 \frac{e \dot{e}_m}{1 - e^2} - 2 \frac{\dot{M}_{L1}}{M_p}. \quad (95)$$

Unless the planets have very small a 's, the matter lost from their Roche lobe cannot directly strike the surface of the host star, and it forms a circumstellar disk. During its infall onto and subsequent viscous evolution within the disk, both energy and angular momentum are tidally transferred between the overflow gas and the planets' orbits. Unless the net energy and angular momentum transfer rates are exactly balanced, eccentricity of the planet may be modified at a rate $\dot{e}_m/e = \eta \dot{M}_{L1}/M_p$. The actual magnitude and sign of η is determined by the combined and competing effects of corotation versus Lindblad resonances (Goldreich & Tremaine 1980). Despite the mass transfer, the binary stars' orbits in cataclysmic variables remain circular, which implies that the magnitude of \dot{e}_m is negligibly small compared with that due to the tidal circularization in equation (13). For the remaining discussions, we neglect the contribution associated with \dot{e}_m .

The semi-major axis of an eccentric orbit would shrink due to tidal orbital circularization at a rate $\dot{a}_e = 2ae\dot{e}/(1 - e^2)$ (see eq. 21). This effect of circularization on a is more prominent for larger e , which would be the case for extrasolar planets. The transfer of angular momentum between the planet's orbit and the stellar spin also introduces $\dot{a}_e = 2a\dot{J}_*/J_o$ (see eq. 20) which is generally much smaller than that induced by mass loss or orbital circularization. Finally, the planets' tidal interaction with their residual nascent disk also contributes to inward migration on a time scale τ_d . Consequently, the total change of a comes from these three effects:

$$\frac{\dot{a}}{a} = \frac{\dot{a}_m + \dot{a}_e}{a} = -2 \frac{\dot{M}_{L1}}{M_p} + 2 \frac{e\dot{e}}{(1 - e^2)} + 2 \frac{\dot{J}_*}{J_o} - \frac{1}{\tau_d}. \quad (96)$$

The above equation, together with equation (89), implies that the Roche lobe changes at a rate

$$\frac{\dot{R}_L}{R_L} = -\frac{5\dot{M}_{L1}}{3M_p} - \frac{\dot{e}}{1 + e} \quad (97)$$

where we have neglected the effects of stellar spin synchronization and planet-disk tidal interaction. The first term on the right hand side of the above rate equation indicates that the retreat of the planet’s orbit due to mass overflow would enlarge the Roche lobe. On the other hand, the shrinkage of the planet’s orbit due to orbital circularization would reduce the Roche lobe in size as is indicated by the second term.

In a mass transfer equilibrium, we find, from equations (69), (90), (91), (92), and (97), the mass transfer rate via the L1 point to be

$$\dot{M}_{L1} = -\frac{\lambda M_p}{(1 + 5\lambda/3)} \left(\frac{\dot{R}_p}{R_p} + \frac{\dot{e}}{1 + e} \right). \quad (98)$$

Since λ is positive and greater than unity, the magnitude of \dot{M}_{L1} is significantly reduced from that of $\dot{M}_a(U(L1))$.

5. Mass and dynamical evolution due to Roche lobe overflow

The discussions in the two previous sections indicate that the evolution of M_p , e , and a are closely connected to each other. In this section, we present analytic approximations to assess the dynamical evolution and the outcome of planets which undergo tidal inflation instability.

5.1. Five stages of planets’ tidal inflation

For illustration purposes, we divide the evolution into five stages.

Stage 1: Runaway inflation. We consider a planet with an initial semi major axis a_i , eccentricity e_i , and radius R_i , so that its initial angular momentum is $J_i = M_p(GM_*(1 - e_i^2)a_i)^{1/2}$. These parameters are determined by processes which brought the planets to the vicinity of their host stars. For example, during the epoch of planet formation, young solar type stars may have a radius 2-3 R_\odot so that the planet-star and planet-disk interaction would lead to a halting radius in equation (22) $a_i = R_{\text{halt}} \sim 0.01 - 0.05$ AU. Or if planets are scattered to the vicinity of their host stars, their a_i and e_i may be relatively large but their periastron distance may be only a few stellar radii.

Provided $R_i < R_c \simeq 2R_J$, the necessary and sufficient conditions for tidal inflation instability are, $e_i > e_R(R_c) > e_L(R_c)$ for $a_i < a_{RL}(R_c)$ (see eq. 51) and $e_i > e_L(R_c) > e_R(R_c)$ for $a_i > a_{RL}$. For $R_i > R_c$, these conditions are $e_i > e_R(R_i) > e_L(R_i)$ for $a_i < a_{RL}(R_i)$ and $e_i > e_L(R_i) > e_R(R_i)$ for $a_i > a_{RL}(R_i)$. Unstable planets with $a_i < a_c$ overflow their Roche lobe prior to runaway inflation whereas those with $a_i > a_c$ undergo runaway inflation to overflow their Roche lobe.

These criteria for runaway tidal inflation are derived under the assumption that e is not damped significantly as the planets adjust their sizes toward R_c . This approximation is generally

adequate for $e \gg e_R$. But if e is marginally larger than e_R initially, it may be damped by a non negligible amount and become stabilized before R_i can reach R_c . Such a possibility is best analyzed numerically (see §6).

The dimensionless expansion rate

$$\frac{\dot{R}_p}{R_p} \approx \left(\frac{e_L^2 - e^2}{e_R^2} \right) \left(\frac{\dot{e}}{e} \right) \quad (99)$$

is obtained from equation (35) by interpreting \dot{R}_p as the adjustment rate of the planets' half-mass rather than the Roche radius. Note that strictly speaking, e_L in the above equation should not be the value related to \mathcal{L}_e as shown in eq(48) but the value related to \mathcal{L} . However, our internal structure code indicates that $\mathcal{L} \simeq \mathcal{L}_e$ for a given R_p and M_p , and we adopt this assumption hereafter in this section. Equation (99) is appropriate for all R_p and a 's. For $e > e_R$, the planets' radius adjustment time scale, $\tau_R = R_p/|\dot{R}_p| < \tau_e$ at the onset of tidal inflation. Since τ_R is a rapidly decreasing function of R_p and the planets' semi major axes evolve only after they overflow their Roche radius, the duration of stage 1 is determined by τ_R with $R_p = R_i$ such that

$$\tau_1 \simeq \tau_R(a_i, R_i) = \frac{R_i}{\dot{R}_p(a_i, R_i)} = 10 \left(\frac{e_R^2}{e_L^2 - e^2} \right) \left(\frac{Q'_p}{10^6} \right) \left(\frac{M_p}{M_J} \right) \left(\frac{M_\odot}{M_*} \right)^{3/2} \left(\frac{a}{0.04 \text{ AU}} \right)^{13/2} \left(\frac{2R_J}{R_i} \right)^5 \text{ Myrs.} \quad (100)$$

which, for $R_i \sim R_c \sim 2R_J$, is longer than the expected values of $\tau_d (\sim 10^{5-6} \text{ yrs})$. Thus, it would be a reasonable approximation to neglect the effect of planets' tidal interaction with the disk if they have already terminated their accretion and contracted to $< 2R_J$ when they migrated to the proximity of their host stars. However, if the protoplanets' orbital migration, induced by their interaction with the disk occurs on a time scale which is comparable to or shorter than that for them to contract (Trilling *et al.* 1998), they may reach the vicinity of their host stars with $R_p \sim 2R_J$.

Equation (100) indicates that stage 1 could be completed for those planets which migrated to $a < 0.04 \text{ AU}$ while their host stars evolved through the classical and weak-line T Tauri phases. At the end of stage 1, the tidally inflated planets lose mass through Roche lobe overflow (see stage 2 below). All the metal-rich planetary tidal debris flowing out of the L1 point is accreted by the host stars and thoroughly homogenized in their surface convective envelopes. Early planetary disruption and stellar accretion is unlikely to significantly modify the metallicity of the host stars' convection zone because it is extensive. But $\tau_1 > 10^7 \text{ yrs}$ for planets which terminated their migration at slightly larger radii (at $a > 0.05 - 0.06 \text{ AU}$). In this limit, the onset of the planets' Roche lobe overflow is delayed until their host stars have fully evolved onto the main sequence. For example, the total mass of the surface convection zone of a G dwarf host star is reduced to an asymptotic value of $\sim 0.02M_\odot$ after $\sim 30 \text{ Myr}$ (Ford *et al.* 1999). Thereafter, the accretion of the metal-rich tidal debris from the Roche-lobe overflowing Jovian-mass planets may significantly contaminate the outer regions of their host stars. Most planet-bearing stars are observed to have metallicity higher than the field stars (Gonzales & Laws 2000).

Stage 2: *Orbital evolution of Roche-lobe filling planets* ($e^2 - e_L^2(R_L) > e_R^2(R_L)$). After filling its Roche lobe, an inflated planet continues to expand and to lose mass through both L1 and L2 points at a rate

$$\frac{\dot{M}_{L2}}{M_p} = -\frac{\lambda}{(1 - \lambda/3)} \left(\frac{\dot{R}}{R_p} + \frac{\dot{e}}{1 - e} \right). \quad (101)$$

with $\dot{a} \simeq 0$ if their $a_i < a_{L2}$ (see eq. 93). But, for $a_i > a_{L2}$ the mass loss and migration rates are

$$\frac{\dot{M}_{L1}}{M_p} = -\frac{\lambda}{(1 + 5\lambda/3)} \left(\frac{\dot{R}_p}{R_p} + \frac{\dot{e}}{1 + e} \right) \quad (102)$$

$$\frac{\dot{a}}{a} = 2 \frac{e\dot{e}}{(1 - e^2)} - 2 \frac{\dot{M}_{L1}}{M_p} \quad (103)$$

(see eqs. 98 & 96). Note that negative values of \dot{M}_{L1} correspond to outflow. Since accretion cannot occur in this context, \dot{M}_{L1} must be set to zero if the right hand side of equation (101) or (102) becomes positive.

Neglecting the effect of e excitation due to planets' interaction with the disk and the dissipation within the stellar interior, the rate of e damping is

$$\frac{\dot{e}}{e} = -\frac{21\pi}{3^{2/3} 2 Q'_p} \left(\frac{M_p}{M_*} \right)^{2/3} \frac{1}{P} \quad (104)$$

for both limits (see eq. 13). The dimensionless expansion rate in equation (99) implies that, regardless of the mass loss, the expansion of the inflated planets continues provided their $R_e > R_L$ (negative values of \dot{R} correspond to contraction.) Note that for $e > e_R$, the planets' radius adjustment time scale, $\tau_R = R_p/|\dot{R}_p| < \tau_e$ at the onset of tidal inflation. Since $e_R \propto R_p^{-1/2}$, these inequalities are preserved as the planets inflate and fill their Roche radius. For planets with $R_p = R_L$,

$$e_R(R_L) \simeq 0.1 \left(\frac{q_p/\beta}{0.75} \right)^{1/2} \left(\frac{M_p}{M_J} \frac{M_\odot}{M_*} \right)^{1/3} \quad (105)$$

which is roughly $\propto a^{-1/6}$ according to eq(103) and therefore is weakly dependent on a . On the other hand,

$$\begin{aligned} e_L(R_s = R_L) &= \frac{0.056}{26^{(5-\gamma)/6}} \left(\frac{Q'_p}{10^6} \frac{\mathcal{L}_o}{10^{-6} L_\odot} \right)^{1/2} \left[\frac{M_\odot}{M_*} \left(\frac{a}{0.04 \text{AU}} \right)^3 \right]^{(5+2\gamma)/12} \\ &\simeq \frac{27.4^{\gamma/6}}{263.9} \left(\frac{Q'_p}{10^6} \frac{\mathcal{L}_o}{10^{-6} L_\odot} \right)^{1/2} \left(\frac{P}{3 \text{days}} \right)^{(5+2\gamma)/6} \end{aligned} \quad (106)$$

where the rough approximation is made that the planet is in thermal equilibrium. For a $M_p = 0.63 M_J$ planet (with $\gamma = 3$, $\mathcal{L}_o = 10^{-6} L_\odot$, and $R_p = R_L$),

$$e_L(a, R_L) = 0.02 \left(\frac{Q'_p}{10^6} \right)^{1/2} \left(\frac{P}{3 \text{days}} \right)^{11/6}. \quad (107)$$

which is $\propto a^{11/4}$.

During stage 2, $e^2 - e_L^2(R_L) > e_R^2$ so that \dot{R}_p and \dot{e} have opposite signs, *i.e.* eccentricity damping leads to further inflation. Consequently, the planets are inflated to fill their Roche radius. In addition, the magnitude of τ_R is smaller than that of τ_e , *i.e.* the planets' size adjusts faster than their eccentricity changes. For large e_i ($\gg e_R(a_i)$ and $\gg e_L(a_i)$), equation (99) implies negligible changes in e from e_i while a sizable fraction of M_p is lost and a is increased significantly. But for e_i marginally larger than $e_R(a_i)$ and $e_L(a_i)$, the planets' tidal inflation and mass loss is accompanied by an e reduction by a comparable fraction.

Note that if mass loss does not significantly modify a , as is the case for $a_i < a_{L2}$, e_L would remain constant. Consequently, the stage of runaway inflation continues until the planets are disrupted locally. But for $a_i > a_{L2}$, most of the mass is lost through the L1 point while both a and $e_L(R_L)$ increase.

At the end of stage 2, $e^2(a_L) = e_R^2(R_L) + e_L^2(a_L, R_L)$ which occurs at $a = a_L$ (see expression for a_L and the corresponding period P_L in the discussion for stage 3 below). While mass transfer is sustained, equations (99), (102), and (103) implies that

$$\frac{\dot{a}}{a} = \left(\frac{2e^2}{1-e^2} + \frac{\lambda}{(1+5\lambda/3)} \left(\frac{e_L^2 - e^2}{e_R^2} + \frac{e}{1+e} \right) \right) \frac{\dot{e}}{e} \sim \frac{\lambda}{(1+5\lambda/3)} \left(\frac{e_L^2 - e^2}{e_R^2} \right) \frac{\dot{e}}{e} \quad (108)$$

$$\frac{\dot{M}_L}{M_p} = -\frac{\lambda}{(1+5\lambda/3)} \left(\frac{e_L^2 - e^2}{e_R^2} + \frac{e}{1+e} \right) \frac{\dot{e}}{e} \quad (109)$$

Since $\lambda \sim 3$, τ_M and τ_a are $< \tau_R$, but comparable to τ_e which is an increasing function of a and P . Thus, the duration of stage 2 is

$$\tau_2 \sim \tau_e(a_L, R_L) = 0.44e^{6/11} \left(\frac{Q'_p}{10^6} \right)^{8/11} \left(\frac{M_*}{M_\odot} \right)^{2/3} \left(\frac{M_J}{M_p} \right)^{2/3} \text{ Myr.} \quad (110)$$

which is much shorter than the duration of stage 1, *i.e.* $\tau_1 \simeq \tau_R(a_i, R_i)$.

Thus, runaway tidally inflation requires a substantial lead-in time which is followed by a brief expansion and orbital migration phase. Because they are substantially inflated, the theoretical probability that the transit of Roche-lobe overflowing planets in front of their host stars are observable by distant observers is

$$P_{t2} \simeq \frac{\pi R_* + R_L(a)}{2a} > \left(\frac{M_p}{3M_*} \right)^{1/3} \quad (111)$$

which is larger than for the present day short-period planets due to the enlarged sizes of both R_* (for $\tau_1 < 10$ Myr) and R_p . The actual probability of observing such events may be much smaller because 1) only a small fraction of stars have short-period planets and 2) the duration of this Roche-lobe overflowing stage 2 is brief compared with the life span of the stars. Note that during the transit, the host stars' magnitude is reduced by $\Delta m_t \sim 5 \log_{10}(R_p/R_*)$ which for

the Roche-lobe overflowing planets may be substantially larger than the present-day short-period planets.

Stage 3: *Stagnation and eccentricity damping* ($e_R^2(R_L) > e^2 - e_L^2(R_L) > 0$). The discussion below on stages 3-5 is relevant only for the cases with $a_i > a_{L2}$. Although the magnitude of the e reduction depends on the initial conditions, $e_L^2(a, R_L)$ increases monotonically to $e^2 - e_R^2(R_L)$ such that

$$\frac{e_i^2}{e_L^2(a_i, R_c)} \left(\frac{e^2(a_L) - e_R^2(R_L)}{e_i^2} \right) = \frac{e_L^2(a_L, R_L)}{e_L^2(a_i, R_c)} \simeq \left(\frac{a_L}{a_i} \right)^{15/2} \left(\frac{R_c}{R_L(a_L)} \right)^{5-\gamma}. \quad (112)$$

In deriving the above equation, we ignore the slight dependence of \mathcal{L}_0 on M_p for the simple illustration. Note that $e_R(R_L)$ weakly depends on a (see eq 105) and it is less than $e_R(R_c)$ (see eq. 46). The onset of tidal inflation instability also requires $e_i > e_L(a_i, R_c)$ so that the left hand side of equation (112) is greater than unity. For a $M_p = 0.63M_J$ planet ($\gamma = 3$),

$$a_L = 0.17 \left(e^2(a_L) - e_R^2(R_L) \right)^{2/11} \left(\frac{M_*}{M_\odot} \right)^{1/3} \text{ AU} \quad (113)$$

with a corresponding period

$$P_L = 25.5 \left(e^2(a_L) - e_R^2(R_L) \right)^{3/11} \left(\frac{10^6}{Q'_p} \right)^{3/11} \text{ days}. \quad (114)$$

In the limit $e_i \gg e_R(R_L)$, the planet's e retains its initial magnitude e_i when the above conditions are established so that $a_L \simeq 0.17e_i^{4/11} (M_*/M_\odot)^{1/3} \text{ AU}$, and $P_L = 25.5e_i^{6/11} (10^6/Q'_p)^{3/11}$ days. But, for e_i marginally larger than $e_R(R_c)$ and $e_L(R_c)$, $a_L \sim a_i$, *i.e.* the planets would not migrate significantly before its tidal inflation is stalled.

As $e^2 - e_L^2(R_L) - e_R^2(R_L)$ reduces to just below zero, τ_R becomes long compared with τ_e , although the planet continues to expand provided $e > e_L(R_L)$. But, the reduction of e also leads to a reduction in a and e_L . The planet would continue to fill its Roche lobe and retreat in a if $\partial e_L(R_L)/\partial e > 1$. From equation (107), we find

$$\frac{\partial e_L(R_L)}{\partial e} = \frac{\partial e_L(R_L)}{\partial a} \frac{\partial a}{\partial \dot{e}} \quad (115)$$

But, from equations(102), (103), and (99), we find

$$\left(\frac{\dot{a}}{a} \right) = 2 \left(\frac{e^2}{1 - e^2} + \left(\frac{\lambda}{1 + 5\lambda/3} \right) \left(\frac{e_L^2 - e^2}{e_R^2} + \frac{e}{1 + e} \right) \right) \frac{\dot{e}}{e} \quad (116)$$

so that with $e^2 = e_R^2 + e_L^2$,

$$\frac{\partial e_L(R_L)}{\partial e} = \frac{11}{2} \left(\frac{e^2}{1 - e^2} - \frac{\lambda}{(1 + 5\lambda/3)} \frac{1}{(1 + e)} \right) \quad (117)$$

which, for $e < 0.6$, is less than unity, primarily due to the planet’s retreat in a as a consequence of angular momentum conservation. Thus, for modest values of e , the quasi-equilibrium cannot be maintained and e rapidly declines below e_L .

During stage 3 when the planet’s e decreases from $(e_R^2 + e_L^2)^{1/2}$ to e_L , \dot{R}_p remains positive but τ_R is larger than τ_e . For

$$a < a_{RL} \simeq 0.08 \left(\frac{q_p/\beta}{0.75} \frac{10^6}{Q'_p} \right)^{2/11} \left(\frac{M_p}{M_J} \right)^{8/33} \left(\frac{M_*}{M_\odot} \right)^{7/33} \text{ AU}, \quad (118)$$

$e_R > e_L$ so that e decreases by a substantial fraction ($\sim e_R/e_L$), M_p decreases and a increases by a modest amount. But for $a > a_{RL}$, $e_R < e_L$ so that e , M_p , and a do not change significantly during stage 3. The duration of this stage is $\tau_3 \sim \tau_e(a_L, R_L)$, *i.e.* comparable to τ_2 .

From equations (102) and (99) we find that Roche lobe overflow is quenched when

$$e_L^2(R_L) - e^2 + \frac{e}{1+e} e_R(R_L)^2 = 0. \quad (119)$$

For relatively small $e_R(R_L)$, the solution for the above algebraic equation is

$$e = e_t \simeq e_L(R_L) \left(1 + \frac{e_L(R_L)}{2(1+e_L(R_L))} \left[\frac{e_R(R_L)}{e_L(R_L)} \right]^2 \right). \quad (120)$$

The termination of Roche-lobe overflow is the result of two competing processes. The reduction in e leads to decreases in a but an increase in R_L . For $e > e_t$, the expansion of R_p is faster than R_L , and equation (103) corresponds to the conservation of total angular momentum. Thus,

$$M_p(a_t, e_t) = M_i \left(\frac{a_i(1 - e_i^2)}{a_t(1 - e_t^2)} \right)^{1/2} \quad (121)$$

which is the asymptotic mass of the planet. For e slightly less than e_t , the expansion of R_L is faster than R_p . Thereafter, equation (102) is replaced by $\dot{M}_{L1} = 0$ and equation (103) is reduced to a requirement for subsequent a and e to obey the conservation of specific angular momentum, *i.e.* $a(1 - e^2) = a_t(1 - e_t^2)$ where a_t is the semi-major axis when e is reduced to e_t . Because the e range in stage 3 is limited and a_L has a weak e dependence, $a_t \sim a_L$.

Stage 4: Onset of contraction ($e_R^2(R_L) > e_L^2(R_L) - e^2 > 0$). When the planet’s e decreases below $e_L(R_L)$, \dot{R}_p and \dot{e} attain the same sign such that the planet contracts despite the tidal dissipation (see eq. 99). Although $R_L > R_c$ so that the Roche-lobe overflowing planets are unstable, $R_e < R_L$ for $e < e_L(R_L)$, *i.e.* the tidal dissipation can no longer supply adequate flux of energy to counterbalance the radiative losses. In this limit, the planets undergo contraction.

The initial contraction proceeds on a time scale $|\tau_R| > \tau_e$. The reduction in e and R_p quickly break the thermal equilibrium such that $\mathcal{L} \gg -\dot{E}_{\text{tide}}$. In this limit, the contraction time scale

$$\tau_c(R_p) = \left(\frac{e_R}{e_L} \right)^2 \tau_e = \frac{q_p G M_p^2}{\mathcal{L} R_p} \tau_e \sim 1.6 \times 10^8 q_p \left(\frac{2R_J}{R_p} \right)^4 \left(\frac{M_p}{M_J} \right)^2 \text{ yr} \quad (122)$$

for a $M_p = 0.63M_J$ planet (see eq. 42). Equation (102) indicates that the outflow is quenched by the contraction of the planets' R_p despite a reduction in their R_L as a consequence of a reduction. Setting $\dot{M}_{L1} = 0$ in equation (103), the conservation of specific angular momentum $a(1 - e^2)$ implies that \dot{a} has the same sign as \dot{e} and that the subsequent circularization leads to orbital decay.

Since the planet's e is damped before its size is significantly deflated, the duration of stage 4 is $\tau_4 \sim \tau_e(R_L)$ which is also comparable to both τ_2 and τ_3 and the age of typical classical and weak-line T Tauri stars. For $a < a_{RL}$, $e_R(a, R_L) < e_L(a, R_L)$, τ_R remains to be larger than τ_e as e diminishes well below e_R . In this case, the planet retains its extended $R_p (\sim R_L(a_L) 10R_J)$ until its e vanishes on a time scale $\tau_e(a_t, R_L)$ (see eq. 104). The asymptotic value of the semi-major axis is $a \sim a_t(1 - e_t^2)$. The planet's extended size and aspect ratio (~ 0.1) makes it detectable with transit searches among young stellar objects. For $a > a_{RL}$, $e_L(R_L) > e_R(R_L)$ and the initial contraction evolves into a rapid deflation to R_c when e decreases below $(e_L^2 - e_R^2)^{1/2}$. The fractional e reduction is $\delta e/e_L(R_L) \simeq e_R(R_L)^2/2e_L(R_L)^2 < 1$ with a similar change in a . In this case, the duration of stage 4 is $\sim (e_R^2(R_L)/2e_L^2(R_L))\tau_e$.

Stage 5: Runaway deflation and return to stable equilibrium ($e_L^2(R_L) - e^2 > e_R^2(R_L)$). The e damping reduces the energy dissipation rate and the planet's equilibrium radius R_e to be less than R_c or $\sim 2R_J$. For $a < a_{RL}$, e vanishes on a time scale $\tau_e(R_L) \ll \tau_R(R_L) \sim \tau_c(R_L)$. Thereafter, the planet contracts from the Roche radius to R_c on a time scale $\tau_c(R_c)$. Although planets located at $a > a_{RL}$ may retain a substantial $e (\sim e_L(R_L))$ when their $e_L^2(R_L) - e^2 > e_R^2(R_L)$, they also contract to $\sim R_c$ on the time scale of $\tau_R \sim \tau_c(R_c)$. But, since $\tau_e \propto R_p^{-5}$, the e damping time scale for these planets increases rapidly with their contraction.

Since $e_R(R_p) \propto R_p^{-1/2}$ (eq. 46), and $e_L(R_p) \propto R_e^{(\gamma-5)/2}$ (eq. 48), the magnitude of both e_R and e_L increase by the contraction of R_p when $\gamma < 5$ or $R_p > R_c$. As e becomes smaller than e_R and e_L , the effect of tidal heating diminishes monotonically. In both limits, the runaway deflation reduces R_p below $\sim R_c$ on a time scale $\tau_c(R_c) \sim 10^8$ yr which is the duration of stage 5, τ_5 .

After R_p is reduced to $\sim 2R_J$, the planet's contraction slows down. Initially, $\mathcal{L} \gg -\dot{E}_{\text{tide}}$ so that the primary source of energy for the planet's luminosity is the release of gravitational energy. But, this energy release rate decreases with time (Burrows et al. 1997). If e is damped to a negligible magnitude, R_p would contract to become comparable to that of Jupiter today. The retention of any residual e would provide an additional energy source such that the contraction would continue until an energy equilibrium is established and R_e attains the values given by setting $\mathcal{L} = -\dot{E}_{\text{tide}}$ in equation (40).

Associated with this energy dissipation, the planets' e would be dissipated on a time scale $\tau_e(R_e)$ (see eq. 18). But for relatively large a 's and small R_p , τ_e is likely to be much longer than the expected life span of typical solar type stars and e is not significantly damped after stage 4. Similarly, the evolution of the planets' a is also likely to terminate.

5.2. Semi-major axis expansion and mass reduction factor

The final dynamical properties of a tidally inflated planet are determined by the conservation of total angular momentum. The above discussions indicate that unstable planets with $a_i < a_{L2}$ expand to overflow their Roche lobe via both the L1 and L2 points. The planet’s angular momentum is absorbed by the lost mass exterior to the orbit and it become tidally disrupted *in situ*. But, unstable planets with $a_i > a_{L2}$ overflow their Roche radius via the L1 point and they must absorb all the initial angular momentum. In this case, the planets’ mass loss is terminated during stage 3 when they attain a_t and e_t . In the limit that $e_t \ll e_i$, the fractional loss of mass $\Delta M_p/M_p \simeq (a_t - R_i)/2a_L + e_i^2/(1 - e_i^2) \sim 0.05 - 0.3$ (see eq. 121). Most short-period planets are fractionally less massive than the more distant planets, though this trend is probably due to observational selection effects. Nevertheless, the absence of very massive planets among them may be indicative of some mass loss for the short-period planets.

In the above discussions, we show that all planets with $P > P_{eL}(e = 1)$ are stable against runaway tidal inflation. Also no planet can continue to overflow its Roche lobe with $P > P_L(e = 1)$. Nevertheless, $P_L(a_t, e_t)$ can be considerably larger than the circularization period for isolated planets with similar kinematic properties. Equation (18) indicates that the decay time of e would be extremely short owing to large radii (= Roche radii) during overflow phases: in the case that the Roche radius $R_L = 4.92R_J$ at $a = 0.04$ AU at the beginning of overflow, equation (18) gives τ_e as short as $\sim 10^5$ years. When the planets’ mass loss through Roche lobe overflow is terminated at a_L , $\tau_e(a_L, R_L)$ is still less than 1 Myr (see eq. 110). Unstable planets with $a > a_{RL}$ may retain their residual eccentricity. Thus, around stars of similar ages, we expect the coexistence of planets with periods up to 2-3 weeks, some with initially highly eccentric orbits but which migrated outward and therefore currently have circular orbits, and others with orbits in which the planets did not inflate too much and have stayed near their original orbits, with initially and currently modest eccentricity.

In the absence of any tidal heating, protoplanets with $R_p \simeq 2R_J$ overflow their Roche radius when their a is reduced to ~ 0.014 AU. Trilling et al. (1998) suggested that after their tidal interaction with their protoplanetary disks brings them to such a distance from their host stars, protoplanets lose mass primarily through the L1 point. They also proposed that the angular momentum transferred from the lost mass to the remaining protoplanet may be adequate to compensate for the angular momentum loss to the disk. Since this halting mechanism can only occur when the protoplanets overflow their Roche lobe, it is unlikely to be effective for planets with periods greater than 3 days, even taking into consideration their inflation by tidal dissipation. For protoplanets which migrated to such close range, this mechanism alone cannot sustain a protracted angular momentum drainage by a long-lived disk. In the absence of a strong tidal interaction with rapidly rotating host stars or the existence of a cavity in the inner regions of their disks to halt their migration (Lin et al. 1996), all protoplanets that migrate to the close neighborhood of their host stars would perish through tidal disruption.

In view of the uncertainties in the magnitude of Q'_p , we briefly discuss the dependence of various quantities on it. The quantities which linearly vary with Q'_p are the time scale of eccentricity damping and tidal inflation. A relatively large Q'_p can significantly prolong the process of tidal inflation. But, the dependence of the critical eccentricity (e_L) for runaway inflation on Q'_p is more modest. For sufficiently large e 's, the critical values of a 's for the onset of tidal inflation, Roche-lobe overflow, and deflation are relatively insensitive to the magnitude of Q'_p . Since the mass reduction factor is determined by the stalling semimajor axis, it too is an insensitive function of Q'_p . Thus, provided the magnitude of $Q'_p < 10^8$, our overall conclusion that runaway inflation may lead to Roche lobe overflow and the disruption or the displacement of ultra short-period eccentric extrasolar planets does not sensitively depend on the equilibrium tidal prescription we have adopted.

6. Numerical Simulation of Tidal Inflation

The analytic approximations presented in the previous sections are useful for categorizing various potential evolutionary paths. However, the stability criteria in equations (46) and (49) neglect the planets' e damping during their evolution towards a state of thermal equilibrium. The discussion in the previous sections also indicates that depending on the planets' initial conditions, there are many possible evolutionary paths and that therefore some of the analytic approximations may not be appropriate.

In this section, we present numerical solutions to illustrate the tidal evolution of ultra-short period planets. For this quantitative analysis, we consider a simple extrasolar system which consists of a solar-mass star and a Jovian planet with an initially eccentric orbit. The equations governing the time evolution of e , R_p , Ω_p and a involve total energy and angular momentum conservation of the whole system consisting of a giant planet and a sun-like host star. Some simplification has been made in our approach. We do not perform the calculation for the expansion/contraction of a planet that is placed in the Roche lobe potential. Instead, we use the evolution code of BLM for a spherically symmetric, gravitationally isolated giant planet to estimate the evolution of the planet's radius. We include the heating from both tidal dissipation (appropriate for planets with a ranging from 0.02 AU to 0.05 AU) and the stellar irradiation. Several evolutionary calculations are carried out for each value of M_p , for different (constant with time) values of dissipation rates. In each case the evolution is calculated up to a time of several Gyr or until the radius becomes constant at the value corresponding to thermal equilibrium, that is, when the luminosity generated by dissipation equals the luminosity radiated from the interior. From these calculations we generate a table that supplies the relation $\dot{R}_p = f(\dot{E}_{\text{tide}}, R_p, M_p)$. Then we can interpolate/ extrapolate the values of \dot{R}_p from the table by entering it with any dissipation rate \dot{E}_{tide} calculated from either the equation of e -damping (eq. 27 with the synchronization condition: $n = \Omega_p$), or that of synchronization damping (eq. 27 with the condition for a circular orbit: $e = 0$). We do not run the simulation with both synchronization and circularization

heating at the same time. The heating due to synchronization is much smaller than that due to circularization, as roughly estimated in equation (44). This point will be justified by our simulation results in §6.2. In summary, we solve equations (11), (27), (103), (98), and (126) together with the interpolation/extrapolation function $\dot{R}_p = f(\dot{E}_{\text{tide}}, R_p, M_p)$ for time evolution of e , Ω_p , a , R_p , M_p , and \dot{E}_{tide} .

Several cautions need to be addressed with our approach. First of all, since the simulation carried out by BLM does not take into account the planet spin, we do not include the energy \dot{E}_{spin} to calculate \dot{R}_p . In §3.1, we already showed that E_{spin} is smaller than E_{bind} , and therefore ignoring E_{spin} should not influence the internal structure too much. The second caution is that the value of \dot{R}_p in the tables are computed using constant heating rates. In principle, the evolution of stratification of planets due to thermal imbalance in the case of quasi-hydrostatic equilibrium should react differently to different heating methods. In §3.2, we suggest this assumption might be appropriate because much of the gas in giant planet interiors has a highly non-ideal equation of state so that the tidal dissipation mainly leads to temperature increases without any significant changes in the pressure.

Mass loss starts to occur once the photosphere of an inflated planet reaches its Roche radius. Overflow gas would redistribute mass and angular momentum of the whole star-planet binary system and then alter the semi-major axis with time. In our numerical calculations, we assume the planets overflow their Roche lobe via the L1 point only and that the system evolves in a conservative manner. We employ equation (98) to estimate the mass loss rate \dot{M}_{L1} . Our simulations are terminated once $\dot{M}_{L1} > 0$. This situation usually occurs when the planet starts to contract gravitationally due to inefficient tidal dissipation as e drops to low values in our simulations.

6.1. Eccentricity Damping

Table 1 shows the minimal e 's required for a giant planet to reach its Roche lobe. This e is equivalent to e_L in equation (48). While the larger initial planet radii ($R_{p,\text{init}} = 1.8R_J$ for $1M_J$ and $R_{p,\text{init}} = 2.0R_J$ for $0.63M_J$) represent earlier phases of giant planets, the smaller initial radius ($R_{p,\text{init}} = 1.2R_J$) is used as a later phase of a giant planet that already contracted and is reaching thermal equilibrium. In all these models, we set $M_* = 1M_\odot$ and $Q'_p = 10^6$. The data in parentheses are the times taken for the planet to expand from the initial conditions to fill its Roche lobe in units of Myr. This time scale is equivalent to τ_R in equation (45). The table shows that this time scale increases with a , resulting partly from larger τ_e as indicated in equation (18) (i.e. e decays more slowly at larger a due to a weaker tidal effect) and partly from larger R_L at larger a (i.e. a planet requires a longer time to reach the larger Roche lobe at larger a). The e 's for small-size planets are higher than those for large-size planets as a result of larger gravitational binding energy for the planets starting from smaller radii. The same reason explains why planets with a core require larger e 's to reach their Roche radius than planets without a core. The results

of our simulations indicate that a planet of $0.63M_J$ without a core (with a core) at 0.04 AU starting at the critical eccentricity 0.140 (0.156) and $2 R_J$ will reach its Roche radius in about 1 Myr. This time scale is shorter than the one given by equation (45), which can be explained by the steep change of e and R_p as R_p approaches R_L and the reduced gravitational binding energy that needs to be overcome for larger radii.

The results in Table 1 also show the value of the minimum e is inversely proportional to R_p which is in agreement with the expression in equation (48). The weak dependence with M_p is probably associated with \mathcal{L}_o being an increasing function of M_p . Although planets located at larger a 's require larger values of minimal e 's and thereby survive more easily, the minimum value of e increases less rapidly with a than that expressed in equation (48). The minimum values of e 's are generally larger than e_L , especially for small a . For $a < a_{RL}$, the more appropriate condition for planetary inflation is $e > e_R$ (see eq. 51). The numerical results are in good agreement with the expression of e_R in equation (46).

Figure 1 illustrates the time evolutions of e , R_p , a , and \dot{E}_{te} for a coreless planet with an original $M_p = 0.63M_J$, initially located at 0.04 AU (solid lines) and 0.06 AU (dashed lines). Starting with $e \approx 0.14$ ($e \approx 0.26$), the planet at $a = 0.04$ AU ($a = 0.06$ AU) spends $t \approx 1.4$ Myrs ($t \approx 8.2$ Myrs) and then is able to expand up to its R_L at which $\mathcal{L}_e = -\dot{E}_{te}$. After this point, the planet will contract since the dissipation rate \dot{E}_{te} has already decreased with time before the planet's size reaches its R_L as is shown in the lower-right panel of Figure 1. In the case for larger values of a such as 0.06 AU, \dot{E}_{te} starts to increase more slowly than that for smaller a as a result of a longer damping time scale of eccentricities, leading to a slower rate of expansion as shown in the upper-right panel in Figure 1. As long as the initial e_i is large enough for the planet to expand slowly through the initial phase and then is able to get larger, the inflation rate is subsequently enhanced by its larger radius ($\dot{E}_{te} \propto R_p^5$) and smaller gravitational binding energy. The lower-left panel in Figure 1 shows that a decreases with time due to circularization. The critical eccentricity 0.14, calculated by the detailed simulation for a planet of $M_p = 0.63M_J$ at $a = 0.04$ AU as shown in Table 1 and in Figure 1, just coincides with the value $e_R = 0.14$ based on the rough estimate as shown in equation (46), and is larger than the value $e_L = 0.06$ that is estimated based on equation (48) with an extrapolation of BLM's data as described in §3.2.

Based on the physical process that planet mass is lost through L1 (see eq. 98), we calculate the smallest initial e_i 's required for a giant planet to move from its initial orbit with a semi-major axis a_{init} to its final orbit with a semi-major axis a_{final} . The results without a core and with a core are shown in Tables 2, 3, and 4. The mass loss rate is calculated based on equation(98). The data for $\lambda = 1$ and $\lambda = 3$ are very close to the data for $\lambda = 2$. Therefore we only show the results for $\lambda = 2$ in this paper. Giant planets move away from their host stars by receiving orbital angular momentum transferred to them from the overflow gas, and their masses are reduced by a fraction before they become detached from their Roche lobes. The data in bold face as displayed in parentheses show the final masses of giant planets in units of $1M_J$ after their radii become detached from their Roche radius. Typically, M_p is reduced by $\approx 15\%$ to 40% for planets with

initial e 's comparable to the critical values. The surviving mass is expected to be smaller if the planets' initial e 's are larger than the critical values. These minimal e 's depend on the initial conditions: the greater the initial gravitational binding energy (due to smaller radii, larger mass, or the existence of a core), the greater the dissipation, and therefore the larger the e , is needed to inflate the planet to attain the same final condition. For an outward migration from 0.03 AU to 0.04 AU, a planet starting with $1M_J$ and $1.2R_J$ requires $e \gtrsim 0.2$, a planet initially with $1M_J$ and $1.8R_J$ needs $e \gtrsim 0.17$, and a planet with $0.63M_J$ and $2R_J$ should start with $e \gtrsim 0.14$. However, a giant planet of $1M_J$ and $1.8R_J$ originally located at 0.04 AU requires $e \geq 0.204$ (without a core) or $e \geq 0.223$ (with a core) to migrate to 0.05 AU, indicating the trend of difficulty for a giant planet located further away to move outwards by Roche lobe overflow. The difference of critical e 's between a planet with a core and without a core increases with a because weaker tidal interaction occurs at larger a . The first values in parentheses (not in bold face) show the time scale in units of Myrs for a from a_{init} to a_{final} . The time scales range from some small fraction of one Myr to more than 10 Myrs depending on initial values of e , a_{init} , and a_{final} .

Figure 2 displays the time evolution of e , R_p , a , M_p , and \dot{E}_{te} for a planet without a solid core. The initial radius is $1.8 R_J$ and the initial mass is $1 M_J$. Starting with the $e = 0.155$ which is the minimal eccentricity to get to the final orbital distance 0.04 AU as shown in Table 2, the planet reaches its Roche lobe around $t = 0.34$ Myrs, marked by dashed lines in the figure. The beginning of the Roche overflow phase is illustrated in the M_p/M_J vs t plot where M_p starts to fall off around $t = 0.34$ Myrs. At the same time, \dot{E}_{te} reaches the maximal value. Subsequently, the planet loses its mass, moves outwards, and increases its size as a result of Roche lobe overflow. The decrease in \dot{E}_{te} during the overflow phase is a consequence of the increase in a . The mass loss rate is determined by equation (98) with the condition that $\lambda = 2$. After having lost $0.16 M_J$, the planet starts to contract and therefore detaches from its Roche lobe at $a \approx 0.04$ AU due to inefficient \dot{E}_{te} (and e) when $t \approx 0.45$ Myrs. Note that a slightly decreases with time before the beginning of the Roche phase ($t \lesssim 0.34$ Myrs) as a result of orbital circularization. However, the change of a is dominated by the effect of overflow during the mass-losing phase (i.e. $|\dot{a}_m| > |\dot{a}_e|$ in equation (96) when $t > 0.34$ Myrs).

Figure 3 illustrates the evolution of the same planet as shown in Figure 2 but with a larger value of initial eccentricity. With a large value of initial e , the whole dynamical evolution should more or less go through a sequence of the stages as illustrated in §5. Owing to the larger initial $e = 0.2$ shown in Figure 3, the planet loses more mass and therefore migrates even farther out than the case (as shown in Figure 2) with the initial $e = 0.155$. The planet enters its Roche-overflowing phase at $t \approx 0.13$ Myrs. During the period $t = 0.13$ to 0.2 Myrs (i.e. the early phase of the Roche overflow), R_p increases roughly from $4R_J$ to more than $7R_J$ but e declines approximately from 0.14 to 0.12, demonstrating “Stage 2” described in §5. The following phase after $t > 0.2$ Myrs featured by the flattening trend of R_p with time confirms the stagnation stage (i.e. Stage “3”) described in §5. The final contraction stage is not able to be simulated with our method which is based on extrapolation/interpolation of the planet data inflated up to the equilibrium radii.

The above results are based on the assumption that overflow occurs only through the L1 point. However, there might be an additional concern in the star-planet interacting system. The gravitational potential difference between the L1 and L2 points is drastically reduced for the small mass ratio $M_p/M_* \approx 10^{-3}$, therefore raising the possibility of overflow through the outer Lagrangian point (L2). Our simulation for a planet of $1M_J$ without a core at $a = 0.03$ AU shows that for the initial eccentricity $e = 0.155$ ($e = 0.5$), the rate of mass transfer across equipotential surfaces is about $\dot{M}_a \approx 4 \times 10^{17}$ g/s (9×10^{18} g/s), which should be roughly comparable to the mass flux via the L1 point. This flux is given by equation (81). Let us estimate this mass flux \dot{M}_{L1} based on the conditions at the photosphere: $\rho = 10^{-8}$ g/cm³, $c_s = 4 \times 10^5$ cm/s. These values would give rise to the mass loss rate $\dot{M}_{L1} \approx 10^{18}$ g/s. Hence $\dot{M}_{L1} \gtrsim \dot{M}_a$ for initial $e = 0.155$, but $\dot{M}_a \gtrsim \dot{M}_{L1}$ for initial $e = 0.5$. As we discuss in §4, mass should be primarily transferred via the L1 point in the small- e limit since the bottom of the planet’s photosphere underfills the L1 point and the density scale height h_ρ is smaller than ΔD as shown in equation (66). In the large- e regime, the bottom of the planet’s photosphere overfills L1, probably leading to a significant amount mass loss through L2. If the planet starts at $a = 0.02$ AU, our simulation shows that $\dot{M}_a \approx 5 \times 10^{18}$ g/cm³ for initial $e = 0.25$, therefore increasing the chance of overfilling the L1 point as indicated by equation(84) for smaller a .

In the previous section, we suggested that in a system with $2ea < h_\rho$, mass transfer is continuous because the gas removed from the atmosphere is replenished on a dynamical time scale by the requirement of hydrostatic equilibrium. For planets with larger e ’s, the envelope as well as the atmosphere needs to adjust. Also as reasoned in the previous section, the underlying envelope of the planet expands at a rather slow rate, which should not be of importance in determining \dot{M} if there is continuous mass overflow in one orbital period. Our simulation shows that the fastest expansion rate of the planets’ envelope is $\dot{R}_p \sim 0.1$ cm/s for an initial $e = 0.5$, and ~ 0.01 cm/s for an initial $e = 0.155$ in the case of a giant planet of $1M_J$ without a core at $a = 0.03$ AU.

When a planet moves from perihelion to aphelion, its Roche radius increases at a rate

$$\dot{R}_L \approx \left(\frac{M_p}{3M_*}\right)^{1/3} \left(\frac{2ae}{P/2}\right) \sim 10^5 \left(\frac{M_p}{M_J}\right)^{1/3} \left(\frac{M_*}{M_\odot}\right)^{1/6} \left(\frac{0.04\text{AU}}{a}\right)^{1/2} \left(\frac{e}{0.2}\right) \text{ cm/s}, \quad (123)$$

which is indeed much larger than the expansion rate ~ 0.1 cm/s due to the e -damping from our simulation. On the other hand,

$$2ae \approx 1.66 \times 10^9 \left(\frac{e}{0.2}\right) \left(\frac{a}{0.04\text{AU}}\right) \text{ cm} \sim h_\rho \approx 2 - 3 \times 10^9 \text{ cm}, \quad (124)$$

where h_ρ is evaluated at 0.04 AU (see §4.2). As a result, one would expect mass overflow via the L1 point to be sustained in different phases of one orbital period despite the re-expansion of planet’s atmosphere, although the most prominent overflow occurs around the perihelion. Hence we conclude that using the Roche radius based on perihelion is a reasonable approximation for small e ’s. However, h_ρ would be much larger than $2ae$ at smaller a since h_ρ gets larger due to more intensive stellar radiation and furthermore $2ae$ gets smaller.

So far we have not considered the effect of the planet’s tidal interaction with the protostellar disk and the consequent inward migration. The primary concern about inward migration is that if the planets’ orbits are almost circularized by the time they reach $a = 0.04$ AU, tidal dissipation within them wouldn’t be available to inflate their radii. As has been discussed in §3.3, there might be a couple of theoretical mechanisms to excite/damp e as giant planets migrate in through a disk. We do not include these uncertain mechanisms in this paper, but only take into account the damping of e due to \dot{E}_{te} as a function of various inward migration rates, using a simple prescription $a/\dot{a} = \text{constant}$. Figure 4 shows the evolution of e of a coreless synchronized planet, with $1M_J$ and $1.8R_J$, moving toward its host star from $a = 0.4$ AU on three different time scales: $-a/\dot{a} = 5, 1, \text{ and } 0.1$ Myr. The simulations start with $e = 0.2$ and $e = 0.3$ and end before the planet reaches its Roche lobe. As shown in Figure 4, e ’s do not drop noticeably from their initial values until the planet reaches $a = 0.04$ AU; thus at this point enough energy from orbital circularization still remains to inflate the planet to its Roche radius. The orbital distance a for Roche overflow shifts to smaller values when a/\dot{a} or initial e is smaller.

The minimal e ’s listed in the first column (i.e. those data with the initial condition $a_{init} = 0.02$ AU) in Table 4 are unexpectedly large compared with those in the first columns in Tables 2 and 3 when the values of these minimal e ’s are $\gtrsim 0.2$. In principle, an internally-heated planet starting with a smaller mass and a larger size should overcome its gravitational binding energy more easily. In reality, this surprising outcome results from a special initial condition for any large e : the initial radius $R_p = 2R_J$ is already larger than the planet’s Roche radius R_L for $R_p = 0.63M_J$, $a = 0.02$ AU, and $e > 0.2$ according to equation (34). Under such a circumstance, the planet cannot be inflated to a large size before overflow happens, leading to less intensive tidal heating and therefore requiring a larger e to reach $a = a_{final}$. In contrast, a planet at $a_{init} = 0.02$ AU starting with more mass such as $1M_J$ can be inflated to a larger size before overflow starts to take place, resulting in more intensive tidal heating and thereby requiring a smaller e to migrate to the same final location a_{final} .

6.2. Synchronization

In this subsection, we shall show that unlike orbital circularization, synchronization is not a promising source of dissipation for a planet within 0.04 AU of its host star since the planet is almost completely synchronized during the course of its inward migration. In this analysis, we consider the dissipation solely due to synchronization, but including orbital migration and the planet’s inflation/contraction. There will be three equations governing the time evolution of Ω_p , R_p , and a . We employ the same assumptions and approach for evaluating \dot{R}_p and \dot{a} for synchronization damping as we described in the previous section for eccentricity damping. In the case of synchronization for a circular orbit, the dissipation is given by $\dot{E}_{t\Omega}$ in equation (28):

$$\dot{E}_{t\Omega} = \frac{I_p |n - \Omega_p| \Omega_p}{\tau_\Omega} = 2.41 \times 10^{-5} \left(\frac{R_p}{R_J} \right)^5 \left(\frac{0.04 \text{ AU}}{a} \right)^{9/2} \left(\frac{M_*}{M_\odot} \right)^{3/2} \left(\frac{10^6}{Q_p} \right)$$

$$\left[0.34 \left(\frac{M_*}{M_\odot} \right)^{1/2} \left(\frac{0.04 \text{ AU}}{a} \right)^{3/2} - \frac{1 \text{ day}}{2\pi/\Omega_p} \right]^2 L_\odot. \quad (125)$$

In equation (5), $\dot{\Omega}_p$ contains two pieces, each of which is associated with a different physical process: synchronization based on the conservation of orbital and spin angular momentum (e.g. see Murray & Dermott 1999), and inflation/contraction based on the conservation of spin angular momentum such that

$$\dot{\Omega}_p = \dot{\Omega}_{\text{tide}} + \dot{\Omega}|_{I_p \Omega = \text{constant}} = \left(\text{sign}(n - \Omega_p) \frac{1}{\tau_\Omega} - \frac{\dot{I}_p}{I_p} \right) \Omega_p. \quad (126)$$

Figure 5 shows the time evolution of a , Ω_p , r_p , $\dot{E}_{\tau\Omega}$, and the synchronization factor Ω_p/n , for a $0.63 M_J$ planet with three different migration rates $a/\dot{a} = 5, 1, \text{ and } 0.1$ Myr. Initially the planets are fast rotators at a spin period $2\pi/\Omega_p = 2$ days, and they start from 0.4 AU with $R_p = 2R_J$. This corresponds to the condition $\Omega_p/n = 46.48$. Then they migrate until they overflow their Roche radii.

In the beginning the spin periods $2\pi/\Omega_p$ decrease as the planets move in as a result of contraction. The contraction phase continues until the tidal interaction becomes so important that the spin frequencies Ω_p are slowed down by the orbital frequencies n which increase with time due to migration. After n catches up with Ω_p (this occurs around $0.05\text{--}0.1$ AU depending on migration rates) and then becomes larger than Ω_p as a result of continuous migration, the spin periods decrease again mainly due to the fact that Ω_p tries to catch up with n because of synchronization. As a result there are two dissipation peaks due to synchronization during the course of migration as illustrated on the $\dot{E}_{\tau\Omega}/L_\odot$ diagram in Figure 5. The first dissipation peak happens at a relatively large a , when n catches up with Ω_p , and the second peak occurs at a smaller a when Ω_p catches up with n . The second peak has a relatively small amplitude compared to the first peak because the difference between n and Ω_p is small during the second dissipation peak. Therefore, one can essentially state that the system has reached its synchronous state after n catches up with Ω_p at around 0.05 AU. This result is in agreement with the discussion in §3.2.

The continuous contraction as shown in the upper-right panel in Figure 5 is just a result of small $\tau_{t\Omega}$ shown in the lower-left panel in Figure 5. A fast migration rate $a/\dot{a} = 0.1$ Myr is unable to boost tidal dissipation high enough to inflate the planet. The final Roche lobe overflow taking place at $a \approx 0.015$ AU (0.016 AU for $-a/\dot{a} = 0.1$ Myr, 0.015 AU for $-a/\dot{a} = 1$ Myr, and 0.014 AU for $-a/\dot{a} = 5$ Myr) is therefore not due to radius expansion, but due to a decrease of the Roche radius as the planet migrates in. Although the simulation is carried out only for a coreless planet with a relatively small mass $M_p = 0.63M_J$, planets with cores or of larger masses such as $M_p = 1M_J$ are more difficult to inflate to their Roche radii by synchronous dissipation due to their larger gravitational binding energy.

We also plot the evolution of a coreless planet with $0.63M_J$ which is being tidally heated as a result of synchronization, starting without any orbital migration. The result is illustrated in

Figure 6. The planet starts as a rapid rotator with $\Omega_p/n \approx 7.64$ at $a = 0.03$ AU (i.e. $2\pi/\Omega_p = 0.25$ days). This value of Ω_p has been chosen to be sufficiently large for the generation of a substantial amount of $\dot{E}_{t\Omega}$, but small enough to limit E_{spin} to be less than E_{bind} . The synchronization time scale is extremely short: $\tau_\Omega \sim 1000$ yrs according to equation (17) for $M_p = 0.63M_J$, $a = 0.03$ AU, $R_p = 2R_J$, and $2\pi/\Omega_p = 0.25$ days. Figure 6 shows that $\Omega_p/n \rightarrow 1$ within a few thousand years. Consequently, even though the equilibrium radius for the intense initial dissipation rate ($0.01L_\odot$) is $R_p = 2.9R_J$, the planet exhausts its energy source and stops its expansion in a couple of thousand years, well before reaching its Roche lobe. This result confirms the general statement $\tau_{R\Omega} > \tau_\Omega$ as described by equation (44).

7. Summary and Discussion

Based upon interpolation/extrapolation of numerical results of internal structure by BLM, we have demonstrated, analytically and numerically, that giant planets with masses $\leq 1M_J$, initial radius $\approx 1.8R_J$, modest e 's ($\gtrsim 0.1 - 0.22$), and small a 's (< 0.04 AU) are likely to be tidally inflated beyond their Roche lobe as they undergo e damping. These conditions may be slightly modified by their internal structure (with or without cores) and by inward migration due to disk-planet interaction. The subsequent mass loss depends on the modification of the internal structure after these tidally inflated giant planets have lost some of their initial mass. Therefore this adjustment is difficult to estimate through our approach based on the numerical data without mass loss by BLM. The degree of outward migration will determine whether or not this Roche lobe overflow model is likely to be responsible for the lack of giant planets within 0.04 AU. How much mass the planet will lose and how far out the planet will migrate is a matter of competition between several factors. Mass loss increases the expansion rate for a given dissipation rate. Our simulation shows that the planet radius, in this case confined by the Roche radius, increases as the planet gains specific angular momentum from the overflow gas through the L1 point. Increasing the semi-major axis a due to Roche overflow via the L1 point inevitably reduces the internal tidal heating. All of these factors undoubtedly depend on the evolution of the internal structure under the condition of mass loss. Nevertheless, we adopt a simplified method by employing the parameter λ to relate the mass loss rate to the expansion rate of the planet (see eq.(98)). Based on reasonable values of λ between 1 and 3, our results indicate that a planet located at larger a_{init} requires a larger value of critical e to move out to the same a_{final} . The minimal values of e to reach the Roche radius increase rapidly as a_{init} increases from 0.03 AU to 0.05 AU as a natural result of the steep dependence on a for tidal interaction. This result depends very weakly on the magnitude of the highly uncertain value of Q'_p . Therefore, our model suggests that the lack of planets inside 0.04 AU might be explained by outward migration due to Roche lobe overflow rather than extreme mass loss. On the other hand, if the protoplanetary disk is still present, the outward migration could be countered by the inward migration from disk–planet interaction; in this case extreme mass loss could actually provide the explanation. The eccentric orbits $e > 0.2$ of extrasolar Jovian planets are theoretically likely as described in §3.3 and are commonly observed,

except near the host star. Also, we have shown that eccentricity damping before a planet migrates to within 0.04 AU is so small that the mechanism of eccentricity damping can provide sufficient energy to inflate a planet to the Roche radius inside 0.04 AU of its host star. Thus Roche lobe overflow due to eccentricity damping seems to be a reasonable mechanism to explain the apparent lack of giant planets within 0.04 AU based on our approach. Around stars of similar ages, we expect the coexistence of planets with periods up to 2-3 weeks, some with initially highly eccentric orbits but which migrated outward and therefore currently have circular orbits, and others with orbits in which the planets did not inflate too much and have stayed near their original orbits, with initially and currently modest eccentricity.

The amount of mass loss provides an estimate of the metallicity enhancement of the host star, provided that (1) the planet’s envelope is substantially enhanced in metals relative to the stellar metal abundance, and (2) some fraction of the overflow mass is able to accrete onto the star. The internal structure of Jupiter and Saturn is somewhat uncertain (Wuchterl *et al.* 2000) ranging from that with a solid core which contains most of the heavy elements to those where metal-enriched gas is well mixed in the convective envelope. But in both sets of models, the heavy element abundance inside Jupiter and Saturn is thought to be 5-10 times larger than that of the Sun. During the stage 2, if the tidally inflated planets lose most of their mass via the L1 point, all the tidal debris would be accreted by the host stars. But if mass flow occurs through both the L1 and L2 points, the tidally inflated planet would be disrupted rapidly with the tidal debris forming an accretion disk which eventually channels the metal rich gas onto the host star. As long as the stars do not have a deep convective envelope, as is true in the case of early-type stars or during the later evolutionary stages of solar-type stars, the effect of metallicity enhancement should be observable on the stellar surface (Sandquist *et al.* 2002). Further investigation should be carried out to clarify these effects.

Once giant planets inwardly migrate to ≈ 0.04 AU through the planet-disk interaction, their spin frequencies are more or less synchronized with orbital frequencies. In spite of the fact that some dissipation is generated as spin frequencies catch up with orbital frequencies within 0.04 AU as a result of inward migration, our results with different inward migration rates show that the internal tidal damping due to synchronization alone is weak enough that the giant planets contract during their entire evolution. A simulation for a fast-spinning planet at 0.03 AU ($\Omega_p/n \approx 7.64$) with no inward migration due to disk-planet interaction shows that the giant planet still cannot be inflated to its Roche radius, consistent with the relation that $\tau_{R\Omega} > \tau_\Omega$ induced from equation (44). However, planet winds may enhance synchronization heating if they can carry a sufficient amount of spin angular momentum out of the planet, thereby holding the planet out of synchronous rotation. This effect should be considered in the future, in a model perhaps analogous to that of the black widow pulsar (Applegate & Shaham 1994).

The migration model through the planet-disk interaction alone seems to have difficulty in accounting for an over-abundance of lower mass planets at $a < 0.1$ AU (Armitage *et al.* 2002). Although the over-abundance may possibly be a result of observational bias, it could, particularly

near $a = 0.04$ AU, be due to the retreat of Roche-lobe-filling planets from the region inside $a = 0.04$ AU. Whether the paucity of the massive close-in Jovian planets (Zucker & Mazeh 2002) results from our scenario is left undetermined until more simulations are carried out for the close-in planets with $M_p > 1M_J$ (but, see Paetzold & Rauer 2002 and Jiang et al. 2003 for another model). The distribution of giant planets at 0.03 AU has been simulated by Trilling et al. (1998) by taking into account the effect of planet-disk interaction, the tidal torque from a fast rotating star, and Roche lobe overflow, but without considering tidal inflation. The effect of tidal inflation causes giant planets to reach the Roche lobe phase at a larger a .

The expansion/contraction rates \dot{R}_p/R_p used in our simulation are taken from the simulations by BLM which are carried out for constant heating rates. But, the dissipation rates actually increase with time for e larger than the minimal values as a consequence of expansion rates larger than eccentric damping rates:

$$\frac{d\dot{E}_{te}/dt}{\dot{E}_{te}} \approx 2\frac{\dot{e}}{e} + 5\frac{\dot{R}_p}{R_p}. \quad (127)$$

We have used equations (29) and (18) to derive the above equation. Therefore, the minimal values of eccentricities required for planets to reach the Roche limit in our simulations are likely underestimated. However, one thing to keep in mind is that all the uncertainty of tidal friction is hidden in the dissipation quantity Q'_p , and we have assumed that the tidal heating is uniformly distributed in planet interiors. Since tidally inflated planets have radiative envelopes (BLM) and it is the radiative envelopes that respond most to the deposition of thermal energy, the effect of tidal expansion might be enhanced due to more dissipation generated in the radiative envelopes as a consequence of the action of radiative damping on the dynamical tide (Zahn 1977).

The overflow mechanism that we explore in this paper might offer a reasonable explanation for the recent HST observation results on a lack of Jovian planets with orbital periods $\lesssim 4$ days around main-sequence stars in the globular cluster 47 Tucanae (Gilliland et al. 2001). In addition to the breakup of planetary systems during frequent encounters with single stars and binaries in the dense core of 47 Tuc or the scenario that the lack of giant planets results from metal-poor circumstellar disks, eccentricities of planets can get excited after a close encounter (Davies & Sigurdsson 2001) with a binary system. Our simulations show that the minimal eccentricities required for a giant planet of $1M_J$ starting with $1.2R_J$ to move from $a_{init} = 0.04$ AU to $a_{final} = 0.05$ AU is ≈ 0.285 , and that the minimal eccentricity for the same planet but at $a_{init} = 0.05$ AU to reach its the Roche radius is ≈ 0.3 . Therefore, with large eccentricities possibly excited in dense stellar environments, a lack of the Jovian planets with very short periods in 47 Tuc could result from the same effect via Roche lobe overflow caused by sufficient tidal inflation. Further investigation on this topic is ongoing (Oh & Lin 2002). Tidally-inflated Jovian planets in eccentric orbits should produce deep transit light curves with shorter flat bottoms, providing an unique signature for the surveys for transiting hot Jovian planets in young extrasolar systems with spectroscopic follow-ups. However, the possibility of finding these objects in surveys, even conducted in some young open clusters, would be small due to the short time scales of tidal

inflation in our model.

We wish to thank A. Burkert, M. Choi, I. Dobbs-Dixon, R. Klessen, G. Laughlin, J. Lim, R. Mardling, G. Novak, K. Oh, E. Vishniac, and H. Yee for useful conversation and valuable comments. We also thank an anonymous referee for highlighting the uncertainties associated with the Q'_p values. Part of this work was completed when one of us (PG) was a visitor at the UCO/Lick Observatory, and he is grateful to K.-Y. Lo for the support of this project. This work is supported by NSF and NASA through grants AST-9987417 and NCC2-5418.

Table 1. Minimal eccentricities required to reach Roche lobes. The cases without a core (the values before /) and with a core (the values after /) are displayed. The numbers in parentheses are the time taken from the initial conditions to the initial Roche phase.

M_p	$R_{p,init}$	0.02 AU	0.03 AU	0.04 AU	0.05 AU
$1M_J$	$1.8R_J$	0.095(0.08)/0.097(0.07)	0.147(0.49)/0.154(0.41)	0.203(1.89)/0.220(1.61)	0.274(4.44)/0.299(3.51)
$1M_J$	$1.2R_J$	0.129(0.20)/0.129(0.18)	0.183(1.64)/0.192(1.07)	0.252(7.17)/0.284(7.18)	0.313(12.7)/0.385(12.6)
$0.63M_J$	$2.0R_J$	0.055(0.05)/0.055(0.06)	0.101(0.32)/0.103(0.23)	0.140(1.35)/0.156(0.93)	0.195(3.82)/0.228(2.65)

Table 2. Minimal eccentricities for planets of initial $1M_J$ and $1.8R_J$ to migrate outwards from initial separations a_{init} to final separations a_{final} based on the equation (93) with the condition that $\lambda = 2$. The first values in parentheses show the time scales in units of Myrs for a to reach a_{final} from a_{init} . The second values in parentheses, which are in bold face, show the final masses in units of $1M_J$ when planet radii detach from their Roche lobe. The cases without a core (the values before /) and with a core (the values after /) are displayed.

a_{final}	$a_{init} = 0.02$ AU	$a_{init} = 0.03$ AU	$a_{init} = 0.04$ AU
≥ 0.04 AU	0.131(0.19, 0.70)/0.147(0.15, 0.70)	0.155(0.45, 0.84)/0.167(0.36, 0.85)	
≥ 0.05 AU	0.145(0.29, 0.62)/0.170(0.20, 0.62)	0.162(0.45, 0.76)/0.180(0.34, 0.76)	0.204(1.83, 0.87)/0.223(1.45, 0.87)
≥ 0.06 AU	0.152(0.59, 0.57)/0.183(0.47, 0.57)	0.174(0.47, 0.69)/0.199(0.32, 0.69)	0.207(1.69, 0.80)/0.229(1.24, 0.79)

Table 3. Same as Table 2 for a planet of $1M_J$, but with a different initial radius $1.2R_J$. The eccentricities shown here are larger than those in Table 2 owing to the fact that a planet of a smaller size has larger gravitational binding energy.

a_{final}	$a_{init} = 0.02$ AU	$a_{init} = 0.03$ AU	$a_{init} = 0.04$ AU
≥ 0.04 AU	0.157(0.26, 0.69)/0.167(0.20, 0.70)	0.189(1.44, 0.84)/0.200(1.31, 0.85)	
≥ 0.05 AU	0.168(0.36, 0.62)/0.188(0.28, 0.62)	0.195(1.31, 0.75)/0.209(1.05, 0.76)	0.253(7.00, 0.84)/0.285(6.62, 0.81)
≥ 0.06 AU	0.174(0.65, 0.56)/0.199(0.50, 0.57)	0.203(1.18, 0.69)/0.223(0.80, 0.69)	0.255(6.68, 0.79)/0.286(6.17, 0.78)

Table 4. Same as Table 2, but with a different initial planet mass $0.63M_J$ and a different initial radius $2R_J$. The eccentricities shown here are in general smaller than those listed in Table 2 and Table 3 except for the cases starting with $a_{init} = 0.02$ AU.

a_{final}	$a_{init} = 0.02$ AU	$a_{init} = 0.03$ AU	$a_{init} = 0.04$ AU
≥ 0.04 AU	0.124(0.58, 0.44)/0.136(0.27, 0.44)	0.122(0.42, 0.54)/0.137(0.29, 0.54)	
≥ 0.05 AU	0.145(0.87, 0.39)/0.177(0.33, 0.39)	0.135(0.50, 0.49)/0.160(0.33, 0.48)	0.150(1.18, 0.55)/0.173(0.71, 0.56)
≥ 0.06 AU	0.171(1.16, 0.36)/0.232(0.36, 0.36)	0.153(0.31, 0.44)/0.194(0.36, 0.44)	0.159(1.08, 0.51)/0.190(0.60, 0.51)

REFERENCES

- Applegate J. H. & Shaham J. 1994, ApJ, 436, 312
- Armitage, P. J., Livio, M., Lubow, S. H. & Pringle J. E. 2002, MNRAS, 334, 248
- Artymowicz, P. 1992, PASP, 104, 769
- Bodenheimer P., Lin, D. N. C., & Mardling, R. A. 2001, ApJ, 548, 466
- Burkert A., & Lin, D. N. C. 2001, in preparation
- Burrows, A., Marley, M., Hubbard, W. B., Lunine, J. I., Guillot, T., Saumon, D., Freedman, R., Sudarsky, D., & Sharp, C. 1997, ApJ, 491, 856
- Cumming, A., Marcy, G.W., Butler, R.P. 1999, ApJ, 526, 890
- Davies M. B., & Sigurdsson, S. 2001, MNRAS, 324, 612
- Dobbs-Dixon, I., Lin, D. N. C., & Mardling, R. A. 2002, in preparation
- Eggleton, P. P., Kiseleva, L. G., & Hut, P. 1998, ApJ, 499, 853
- Ford, E.B., Rasio, F.A., & Sills, A. 1999, ApJ, 514, 411
- Gilliland, R. L. et al. 2000, ApJ, 545L, 47
- Goldreich, P. & Nicholson, P. D. 1977, Icarus, 30, 301
- Goldreich, P. & Nicholson, P. D. 1989, ApJ, 342, 1079
- Goldreich, P. & Tremaine, S. 1980, ApJ, 241, 425
- Goldreich, P. & Sari, R. 2002, submitted to ApJ
- Gonzales, G., & Laws, C. 2000, AJ, 119, 390
- Goldreich, P. & Soter, S. 1966, Icarus, 5, 375
- Goodman, J. & Oh, S. 1997, ApJ, 486, 403
- Hubbard, W. B. (1984). Planetary interiors. New York, Van Nostrand Reinhold Co.
- Ioannou, P. J. & Lindzen, R. S. 1993, ApJ, 406, 252
- Ioannou, P. J. & Lindzen, R. S. 1993, ApJ, 406, 266
- Ioannou, P. J. & Lindzen, R. S. 1994, ApJ, 424, 1005
- Israelian, G., Santos, N. C., Mayor, M. & Rebolo, R. 2001, Nature, 411, 163

- Jiang, I.-G., Ip, W.-H., & Yeh, L.-C., ApJ, 582, 449, 2003
- Johns-Krull, C. M., Valenti, J. A., & Koresko, C. 1999, ApJ, 516, 900
- Konigl, A. 1991, ApJ, 370L, 39
- Kuchner, M. J. & Lecar, M. 2002, to appear in ApJL
- Lin, D.N.C. 1997, in *Accretion Phenomena and Related Outflows*; IAU Colloquium 163. ASP Conference Series; Vol. 121; 1997; ed. D. T. Wickramasinghe; G. V. Bicknell; and L. Ferrario (1997), p.321
- Lin, D. N. C., Bodenheimer, P., & Richardson, D. C. 1996, Nature, 380, 606
- Lin, D. N. C. & Ida, S. 1997, ApJ, 477, 781
- Lin, D. N. C. & Papaloizou, J. C. B. 1986, ApJ, 309, 846
- Lubow, S. H. & Shu, F. 1975, ApJ, 198, 383
- Lubow, S. H., Tout, C. A., & Livio, M. 1997, ApJ, 484, 866
- Marcy, G. W., Cochran, W. D., & Mayor, M. 2000, in *Protostars and Planets IV*, ed. V. Mannings, A. P. Boss, & S. Russell (Tucson: Univ. Arizona Press), 1285
- Mardling, R. A. & Lin, D. N. C., ApJ, 573, 829, 2002
- Mathieu, R. D., Duquennoy, A., Latham, D. W., Mayor, M., Mazeh, T., & Mermilliod, J.-C. 1992, in *Binaries as Tracers of Stellar Formation*, ed. A. Duquennoy & M. Mayor (Cambridge: Cambridge Univ. Press), 278
- Mathieu, R. D. 1994, ARA&A, 32, 465
- Mayor, M. & Queloz, D. 1995, Nature, 378, 355
- Murray C. D. and Dermott S. F. 1999, *Solar System Dynamics*, Cambridge Univ. Press
- Nagasawa, M., Lin, D. N. C., & Ida, S. 2002, submitted to ApJ
- Oh, K. & Lin, D. N. C. 2002, in preparation
- Paetzold, M. & Rauer, H. 2002, ApJ, 568, 117
- Papaloizou, J. C. B., Nelson, R. P., & Masset, F. 2001, A&A, 366, 263
- Peale, S. J., Cassen, P. & Reynolds, R. T. 1979, Science, 203, 892
- Pollack, J. B., Hubickyj, O., Bodenheimer, P., Lissauer, J. J., Podolak, M., & Greenzweig, Y. 1996, Icarus, 124, 62

- Pringle, J.E. 1985, in *Interacting Binary Stars*, eds J.E. Pringle & R.A. Wade, Cambridge University Press: Cambridge
- Rasio, F. A., Tout, C. A., Lubow, S. H., & Livio M, ApJ, 470, 118, 1996
- Rasio, F. A. & Ford, E. B. 1996, Science, 274, 954
- Sandquist, E. L., Dokter, J. J., Lin, D. N. C., & Mardling, R. A. 2002, ApJ, 572, 1012
- Sandquist, E. L., Taam, R. E., Lin, D. N. C., & Burkert, A. 1998, ApJ, 506L, 65
- Showman, A. P. & Guillot, T. 2002, A&A, 385, 166
- Shu, F., Najita, J., Ostriker, E., Wilkin, F., Ruden, S., & Lizano, S. 1994, ApJ, 429, 781
- Stassun, K. G., Mathieu, R. D., Mazeh, T., & Vrba, F. J. 1999, AJ, 117, 2941
- Takeuchi, T., Miyama, S. M., & Lin, D. N. C. 1996, ApJ, 460, 832
- Terquem, C., Papaloizou, J. C. B., Nelson, R. P., & Lin, D. N. C. 1998, ApJ, 502, 788
- Trilling, D. E., Benz, W., Guillot, T., Lunine, J. I., Hubbard, W. B., & Burrows, A. 1998, ApJ, 500, 428
- Ward, W. R. 1981, Icarus, 47, 234
- Weidenschilling, S. J. & Marzari, F. 1996, Nature, 384, 619
- Wuchterl, G., Guillot, T., & Lissauer, J.J. 2000, in *Protostars and Planets IV*, ed V. Mannings, A. P. Boss, & S. S. Russell (Tucson: Univ. of Arizona Press), 1081
- Yoder, C. F. & Peale, S. J. 1981, Icarus, 47, 1
- Zahn, J.-P. 1977, A&A, 57, 383
- Zahn, J.-P. 1989, A&A, 220, 112
- Zucker, S. & Mazeh, T. 2002, ApJ, 568L, 113

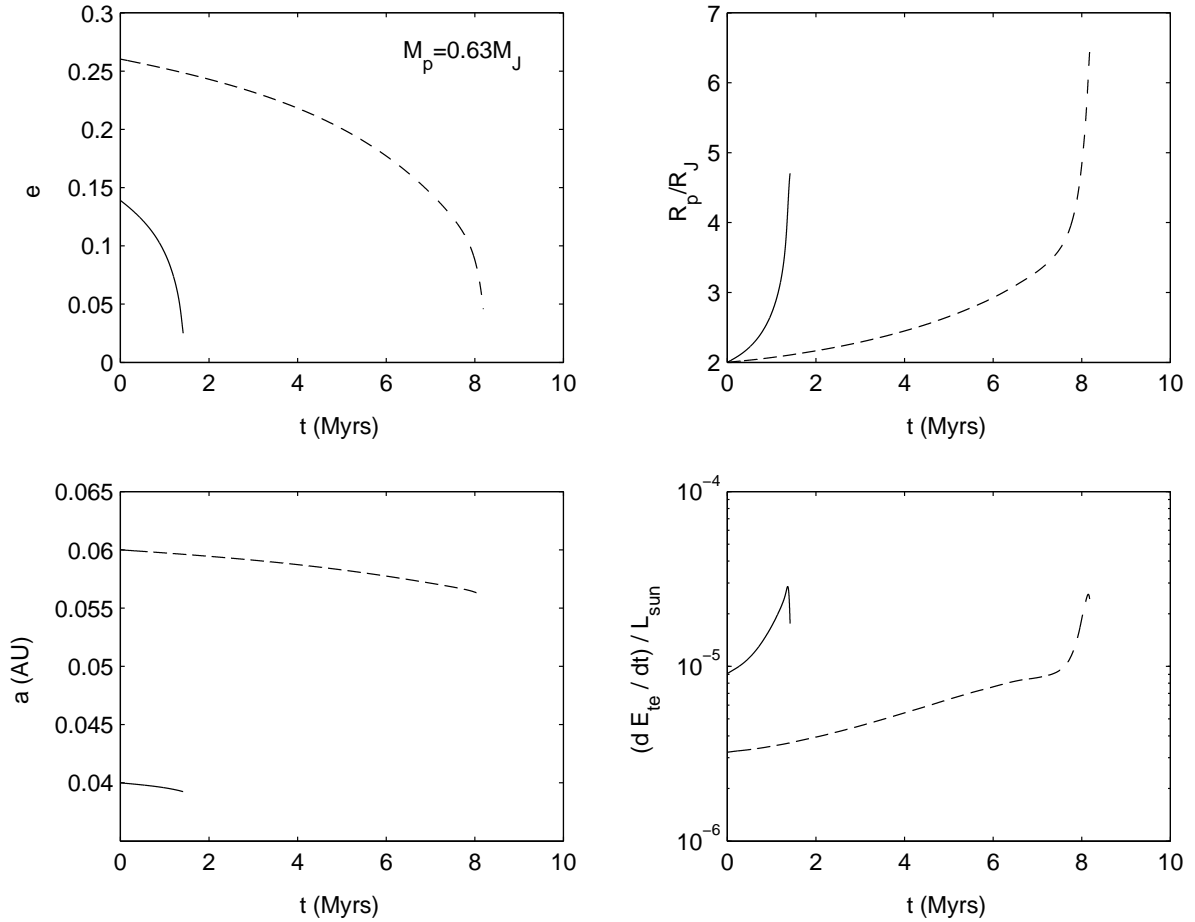


Fig. 1.— Time evolutions of e , R_p , a , and \dot{E}_{te} for a planet of a original $M_p = 0.63M_J$ without a solid core initially located at 0.04 AU (solid lines) and 0.06 AU (dashed lines). Starting with $e \approx 0.14$ ($e \approx 0.26$), the planet at $a = 0.04$ AU ($a = 0.06$ AU) spends $t \approx 1.4$ Myrs ($t \approx 8.2$ Myrs) and then is able to expand up to its equilibrium radius which is just equal to its R_L .

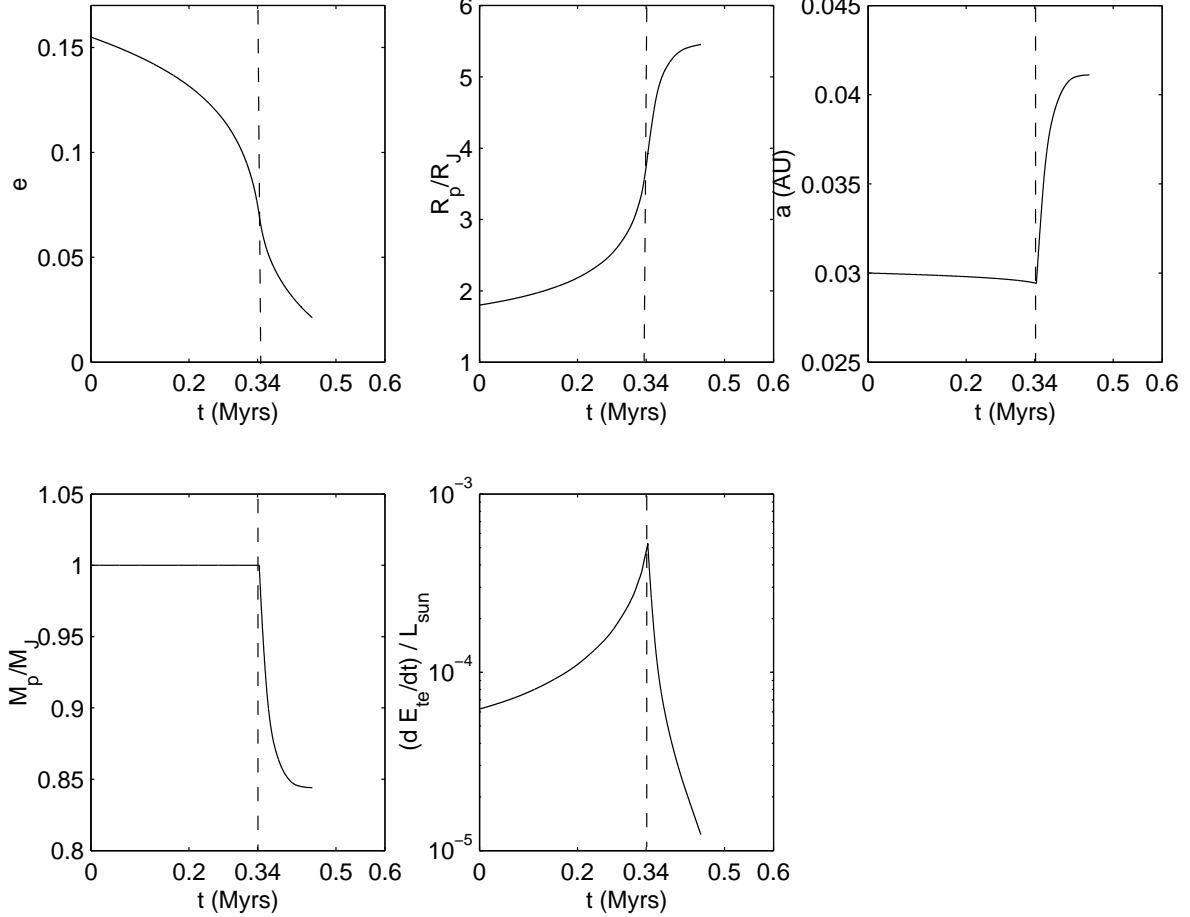


Fig. 2.— Time evolution of e , R_p , a , M_p , and \dot{E}_{te} for a planet with original $M_p = 1M_J$ without a solid core initially located at 0.03 AU. The mass loss is calculated by using equation (98) with the condition that $\lambda = 2$. The moment $t = 0.34$ Myrs marked by a vertical dashed line indicates the beginning of the Roche overflow phase.

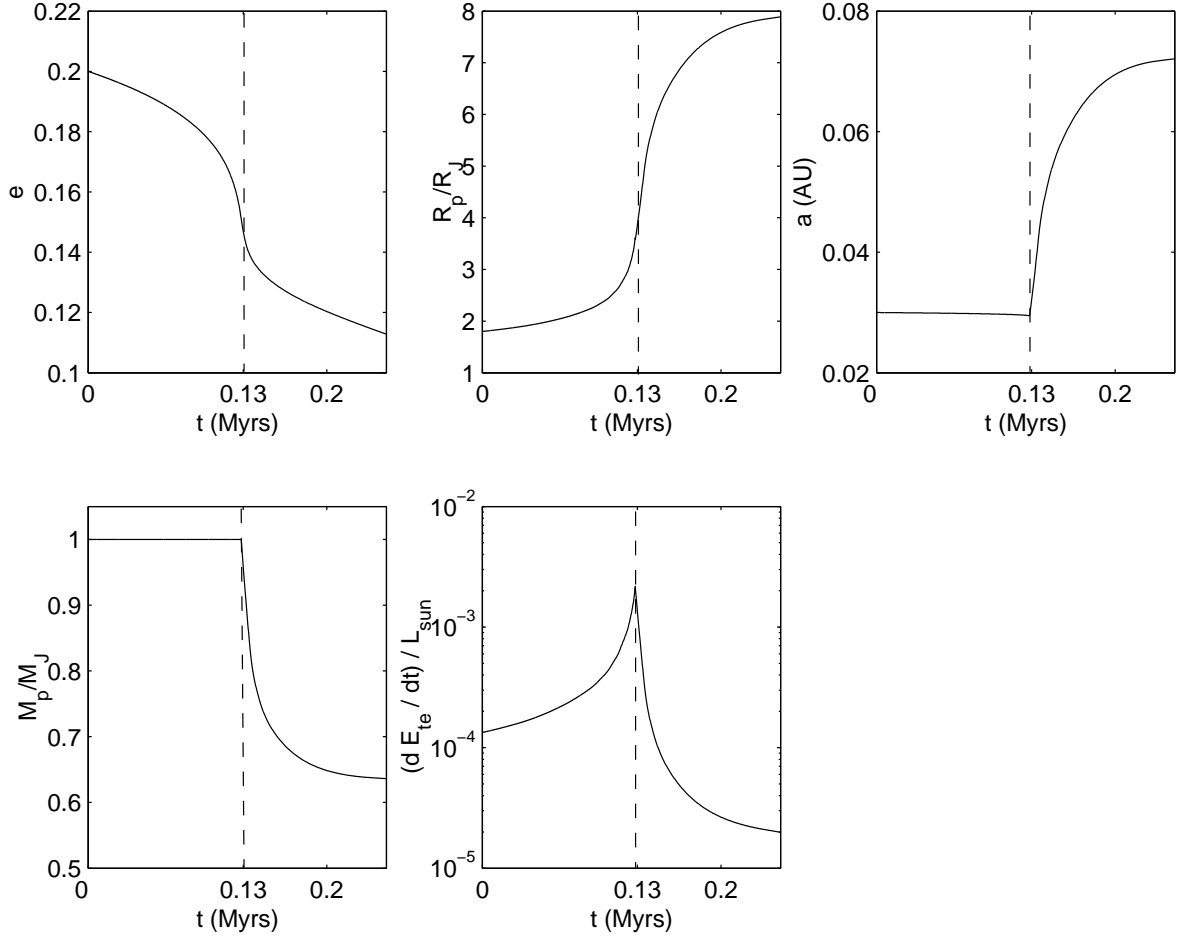


Fig. 3.— The same simulation as the one shown in Fig. 2 except starting with a higher value of $e = 0.2$. The moment $t = 0.13$ Myrs marked by a vertical dashed line indicates the beginning of the Roche overflow phase in this case.

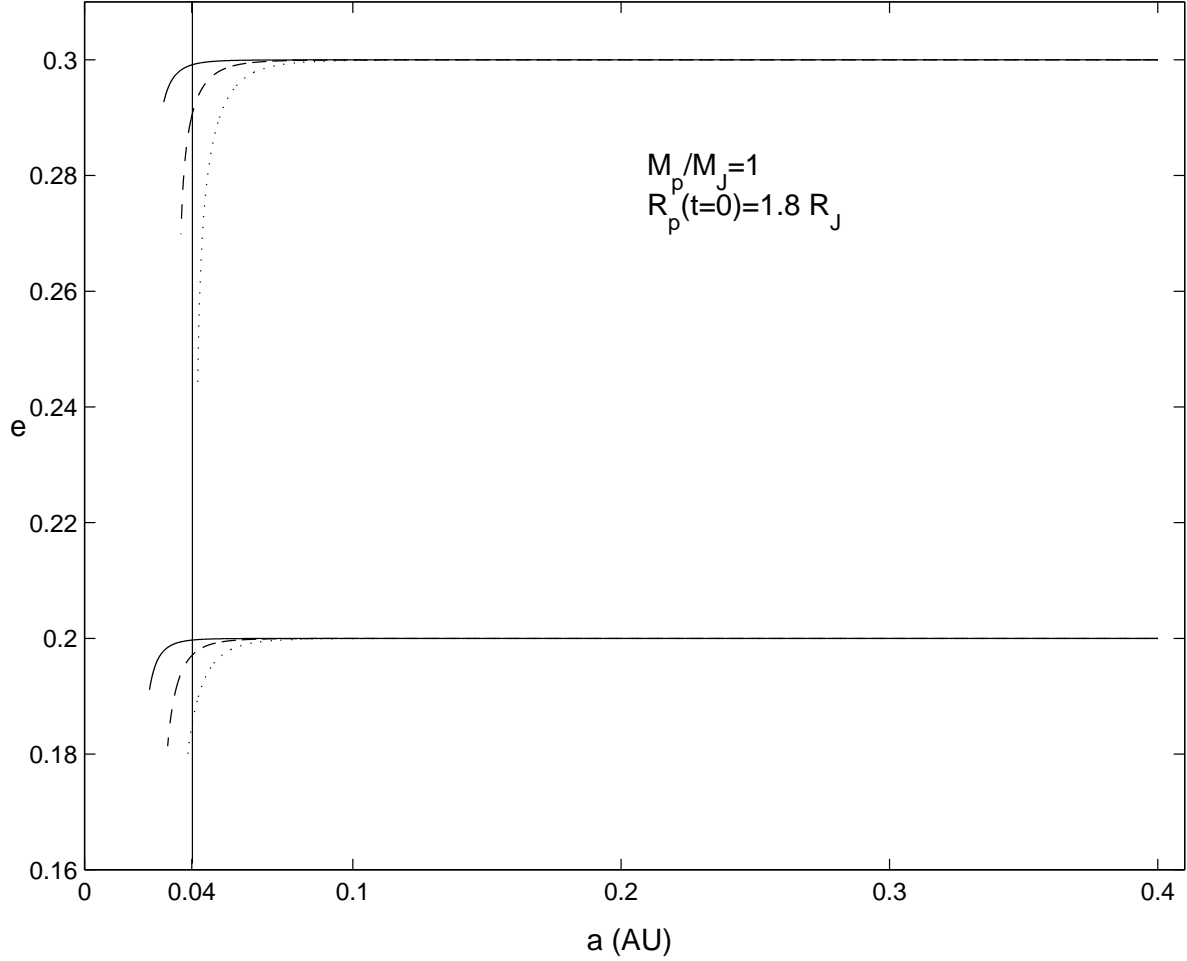


Fig. 4.— Evolution of a for a planet of $1 M_J$ and $1.8 R_J$ without a core and starting at $a = 0.4$ AU, moving inwards at three migration speeds: $-a/\dot{a} = 5$ Myr (dotted lines), 1 Myr (dashed lines), and 0.1 Myr (solid lines). The simulations start with $e = 0.2$ and $e = 0.3$ and end before planets reach their Roche lobes.

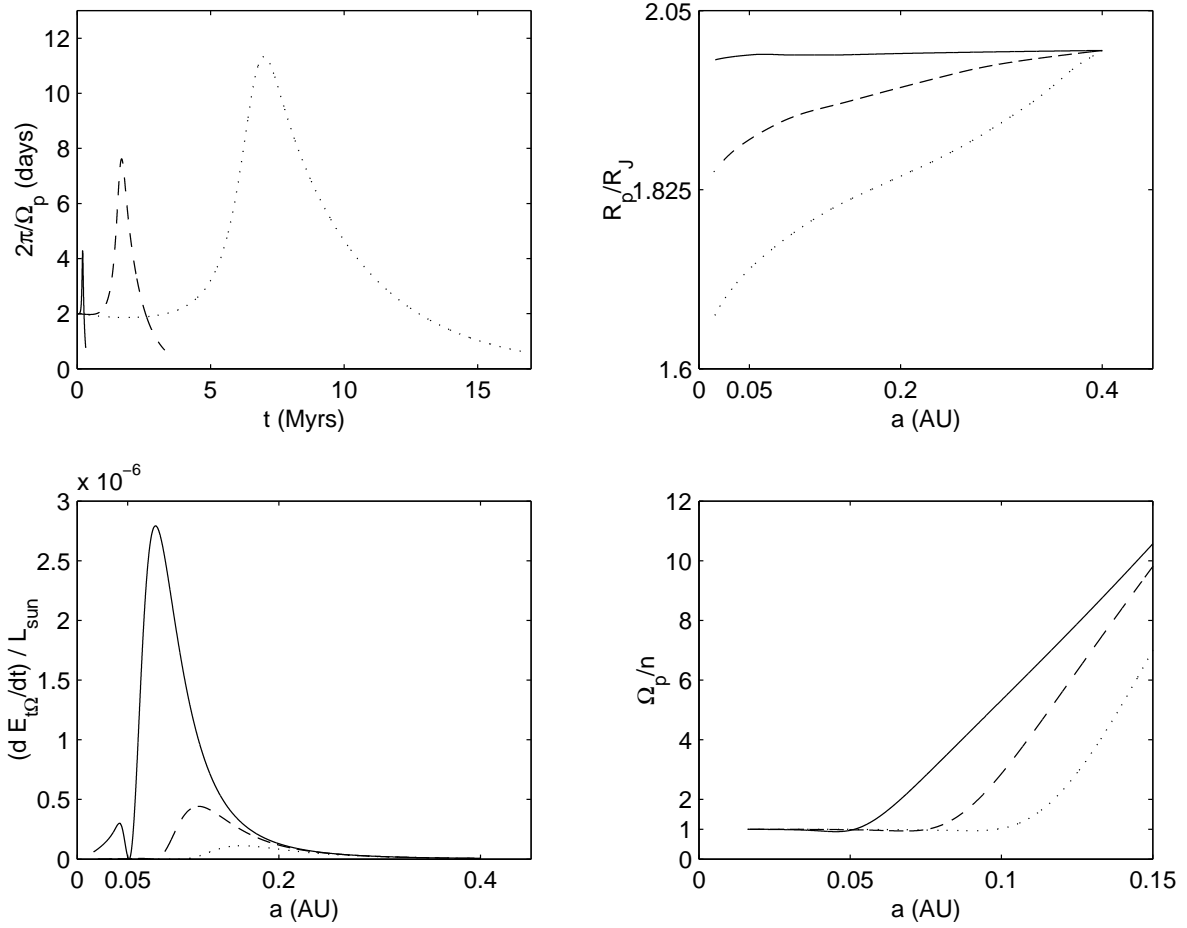


Fig. 5.— Time evolution of Ω_p , R_p , $\dot{E}_{t\Omega}$, and Ω_p/n for a $0.63 M_J$ planet with no core starting from 0.4 AU with three different migration rates: $-a/\dot{a} = 5 \text{ Myr}$ (dotted lines), 1 Myr (dashed lines), 0.1 Myr (solid lines).

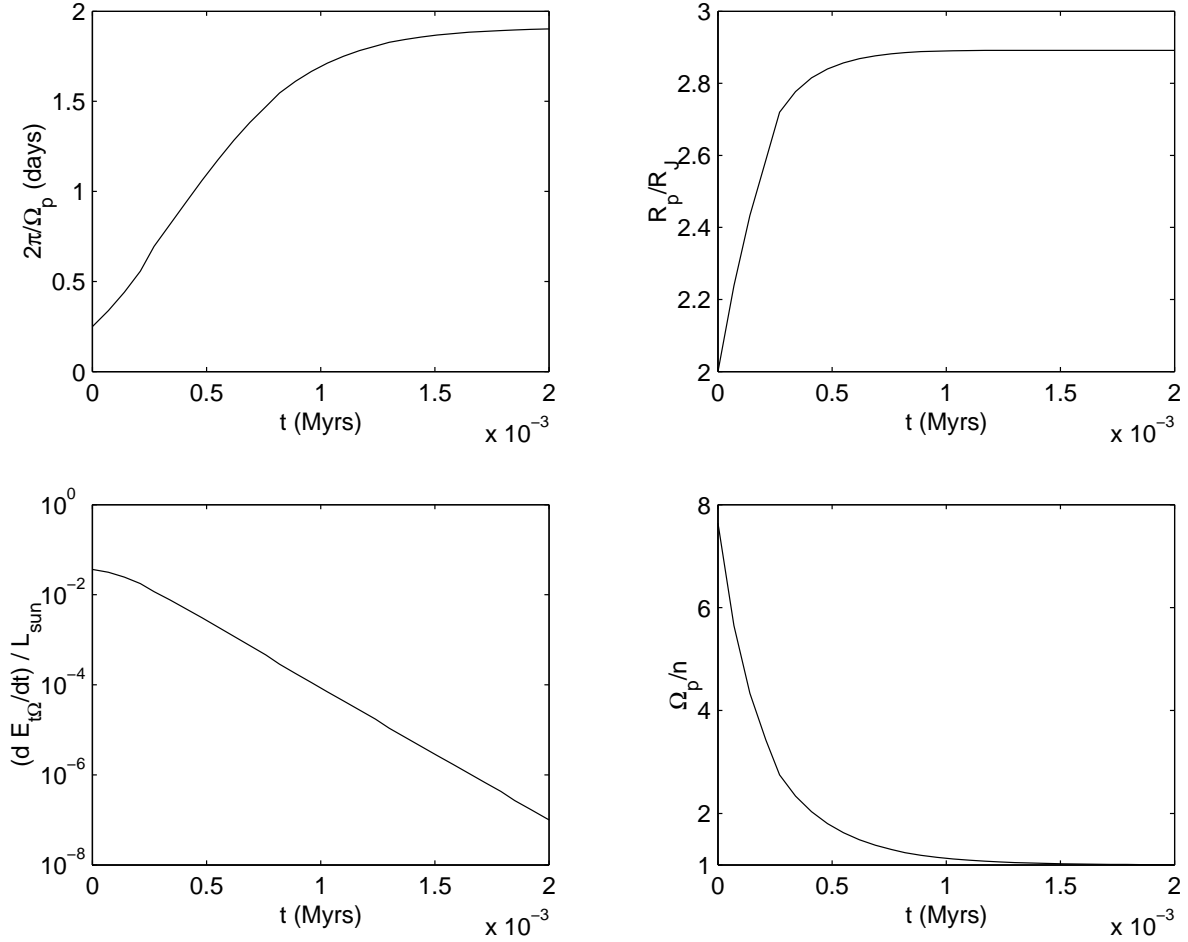


Fig. 6.— Time evolution of Ω_p , R_p , $\dot{E}_{t\Omega}$, and Ω_p/n for a $0.63 m_J$ planet with no core located at 0.03 AU with no migration. The planet starts out as a fast rotator with the ratio $\Omega_p/n \approx 7.64$, and then is rapidly synchronized ($\Omega_p/n \rightarrow 1$) by the tidal effect within several thousand years.